THE JOURNAL OF PHYSICAL CHEMISTRY A

pubs.acs.org/JPCA Article

Modified Density Functional Dispersion Correction for Inorganic Layered MFX Compounds (M = Ca, Sr, Ba, Pb and X = Cl, Br, I)

Published as part of The Journal of Physical Chemistry virtual special issue "Paul Geerlings Festschrift".

Daniel Sethio, João B. L. Martins, Latévi Max Lawson Daku, Hans Hagemann, and Elfi Kraka*

Cite This: *J. Phys. Chem. A* 2020, 124, 1619–1633 Read Online

ACCESS | Metrics & More | Article Recommendations | Supporting Information

ABSTRACT: MFX (M = Ca, Ba, Sr, Pb and X = Cl, Br, I) compounds have received considerable attention due to their technological application as X-ray detectors, pressure sensors, and optical data storage materials, when doped with rare-earth ions. MFX compounds belong to the class of layered materials with a tetragonal Matlockite crystal structure, characterized by weakly stacked double-halide layers along the crystallographic *c*-axis. These layers predominantly determine phase transitions, elastic, and mechanical properties. However, the correct description of the lattice parameter *c* is a challenge for most standard DFT functionals, which tend to overestimate the lattice parameter *c*. Because of the weak interactions between the halide layers, dispersion-corrected functionals seem to be a better choice. We investigated 11 different inorganic layered MFX compounds for which experimental data are available, with standard and dispersion-corrected functionals to assess their performance in reproducing the lattice parameter *c*, structural, and vibrational properties of the MFX compounds. Our results revealed that these functionals do not describe the weak interactions between the halide layers in a balanced way. Therefore, we modified Grimme's popular DFT-D2 dispersion correction scheme in two different ways by (i) replacing the dispersion coefficients and van der Waals radii with those of noble gas atoms or (ii) increasing the van der Waals radii of the MFX atoms up to 40%. Comparison with the available experimental data revealed that the latter approach applied to the PBE (Perdew–Burke–Ernzerhof)-D2 functional with 30% increased van der Waals radii, which we coined PBE-D2* (S_{rvdw} 1.30) is best suited to fine-tune the description of the weak interlayer interactions in MFX compounds, thus significantly improving the description of their structural, vibrational, and mechanical properties. Work is in progress applying this new, computationally inexpensive scheme to other inorganic layered compounds and periodic systems with weakly stacked layers.

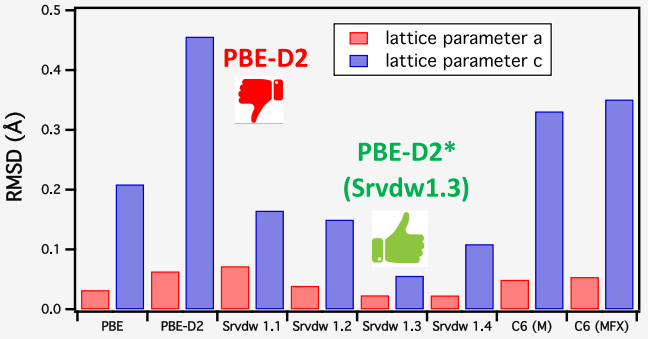

INTRODUCTION

Dispersion forces arising from fluctuating charge distributions have been extensively studied due to their fundamental and technological importance in physics, chemistry, and biology.[1−5] Despite the fact that dispersion energies are more than an order of magnitude smaller than chemical bond energies, the importance of dispersion forces cannot be neglected.[6−10] They are ubiquitous and play a central role, for example, in dictating crystalline structures in solid state systems or in stabilizing the DNA double helix,[11,12] therefore they demand an accurate theoretical description.[3]

Standard density functional theory (DFT) approximations[13−20] poorly describe dispersion forces.[21−23] Local-density approximation (LDA),[24] generalized-gradient approximation (GGA),[25,26] meta-GGA,[27] and also hybrid functionals[28] often lead to remarkable errors in the structures and binding energies of noncovalently bonded dimers, which are known to be held together by dispersion forces.[29−32] This is due to the well-known fact that standard functionals provide an accurate description of short-range electron correlation while they fail describing long-range electron correlation, the origin of long-range dispersion interactions.[33−35] Therefore, the inclusion of dispersion correction into DFT is imperative for the calculation of reliable structural and thermodynamic properties for systems with weak interactions.[36,37]

The development of dispersion-corrected density functionals has been through a long journey.[38,39] Proposed correction schemes range from simpler semiempirical approaches to a complex nonlocal density-based approaches. The five most popular dispersion correction schemes currently in use are (1) C_6-based correction schemes such as Grimme's D2,[40,41] D3,[42] and D4,[43] Tkatchenko–Scheffler's TS,[44] and Becke–Johnson's

Received: November 4, 2019
Revised: December 19, 2019
Published: January 30, 2020

https://dx.doi.org/10.1021/acs.jpca.9b10357
J. Phys. Chem. A 2020, 124, 1619–1633

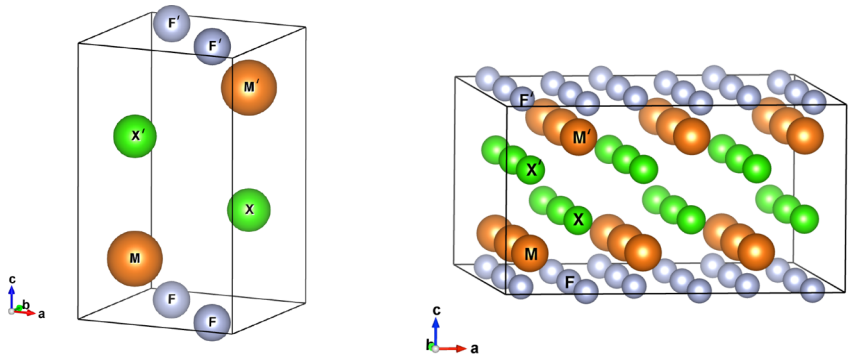

(a) unit cell (b) super cell

Figure 1. Tetragonal *P*4/*nmm* Matlockite structure of MFX (M = M′ = Ca, Sr, Ba, Pb and X = X′ = Cl, Br, I): (a) unit cell and (b) 3 × 3 × 1 super cell showing $-F^{-}-M^{2+}-X^{-}\cdots X'^{-}-M'^{2+}-F'^{-}-$ stacking of the double halide layers along the *c* axis.

XDM schemes;[45] (2) nonlocal density-based functionals such as vdW-DF (2004),[46] vdW-DF2 (2010),[47] rev-vdW-DF2 (2015),[48] VV09,[49] and VV10;[50] (3) dispersion-corrected semilocal functionals such as M06-2X,[27] M08,[51] M11,[52,53] and MN12;[54−56] (4) one-electron effective potentials such as dispersion-corrected atom-centered one-electron potentials (DCACPs)[57−59] and dispersion-corrected potentials (DCPs);[60] and (5) range-separated hybrid functionals such as HSE06,[25,61] HSEsol,[62,63] and ωB97X.[34,64] Among these schemes, the nonlocal density-based functionals, dispersion-corrected semilocal functionals and the range-separated hybrid functionals have the largest numerical complexity, which translates into high computational costs.[65−67] Within the C_6-based schemes, XDM is the most costly method compared to Grimme's D2 and D3 and Tkatchenko's TS schemes.[42,68] Grimme's semiempirical pairwise D2 scheme is one of the most widely used correction schemes.[40,41] DFT-D2 has shown to provide accurate results for molecular complexes.[36,37] However, modifications of original Grimme's parametrization (being originally designed for molecular systems) are frequently required for solid-state studies.[69−75]

MFX compounds have received considerable attention due to their fundamental and technological importance. These compounds, when doped with rare-earth ions, exhibit many interesting properties that have turned out to be useful in applications as diverse as X-ray imaging,[76−79] neutrino detectors,[80] pressure sensors,[81] and optical data storage material.[82] MFX compounds (M = M′ = Ca, Ba, Sr, Pb and X = X′ = Cl, Br, I) crystallized in the tetragonal Matlockite structure with lattice parameters [*a* = *b*, *c*] exhibit a layered ionic structure which corresponds to a simple $-F^{-}-M^{2+}-X^{-}\cdots X'^{-}-M'^{2+}-F'^{-}-$ stacking along the *c*-axis with the presence of double halide layers (see Figure 1).[83−85] At ambient condition, the *c*-axis has a larger compressibility than the *a*-axis, exhibiting quasi-2D character.[86,87] The unit cell consists of two strongly bonded ($-F^{-}-M^{2+}-X^{-}$ and $-F'^{-}-M'^{2+}-X'^{-}$) subunits connected by weak interhalogen $X^{-}\cdots X'^{-}$, M′−X, and M−X′ interactions along the crystallographic *c*-axis.[88,89] In particular, the interactions along the *c*-axis play an important role for the phase transition from *P*4/*nmm* to $P6_3/mmc$ via *Pmcn* under high pressure[86] and determine mechanical and elastic properties as bulk modulus, shear modulus, and Young's modulus for layered materials.[90−92] However, describing the lattice parameter *c* is challenging.[93] Standard DFT functionals such as GGAs (generalized gradient approximation)[25,26] overestimate the lattice parameter *c*.[94−98] To our best knowledge, there are no reports on a systematic study of the performance of dispersion-corrected functionals, which seem to be more suited for the description of the weak interactions along the *c*-axis.

Table 1. Number of Primitive Basis Functions (s/p/d/f) and Their Contraction for the def2-TZVP[104,105] and pob-TZVP[103,106] Basis Sets for MFX (M = M′ = Ca, Sr, Ba, Pb and X = X′ = Cl, Br, I)[a]

	no. of primitives (s/p/d/f) and their contraction	
element	def2-TZVP	pob-TZVP
Ca	8 4 2 111/6 311 1/211	8 4 2 111/6 311/1[c]
Sr	211 111/411 1/111	211 111/411/1[b,d]
Ba	211 111/411 1/311/1	2 111/411/1[b]
Pb	421 111/3 311 1/611/11	4 111/3 311/611[b]
F	6 211 1/411/11/1	6 211/411/1[c]
Cl	7 3 211/5 111 1/21/1	7 3 211/5 111/1[c]
Br	8 4 2 111/6 4 111/511 1/1	8 4 2 111/6 4 111/511 1[c]
I	521 111/3 411 1/611/11	5 111/3 411/611[b,d]

[a]All electron basis sets were used for Ca, F, Cl, and Br while ECP were used for Sr, Ba, Pb, and I. [b]This work. [c]Reference 103. [d]Reference 106.

Therefore, we systematically studied how the PBE functional[25,26] and its dispersion-corrected PBE-D2 form reproduce lattice parameters *a* and *c*, geometries, and vibrational frequencies for a set of 11 different MFX crystals for which experimental data are available. The PBE functional is a well-known nonempirical functional that has proved to be qualified for the description of both molecules and solids.[99−102] We then modified the PDE-D2 functional in order to increase its performance. The results obtained for the most suitable modification derived in this work were compared with some other frequently used dispersion-corrected functionals, including PBE-D3, PBE-TS, PBE-XDM, B3LYP-D*, M06-2X, ωB97X, and HSE06 for three representative MFX compounds.

COMPUTATIONAL METHODS

All geometry optimization and vibrational frequency calculations for the MFX systems investigated in this work were carried out using DFT with periodic boundary conditions based on the PBE functional.[25,26] The pob-TZVP Gaussian-type basis set of polarized valence triple-ζ quality was used for Ca, F, Cl, and Br[103] and consists of highly contracted basis functions for the core−shell, three less contracted basis functions for the valence shell, and one polarization function. This basis set was originally derived from Ahlrichs' def2-TZVP basis set[104,105] by restructuring the contraction scheme and reoptimizing the contraction coefficients of the def2-TZVP basis set.[103,106]

https://dx.doi.org/10.1021/acs.jpca.9b10357
J. Phys. Chem. A 2020, 124, 1619−1633

Table 2. Calculated and Experimental Lattice Parameters of MFX (M = Ca, Sr, Ba, Pb and X = Cl, Br, I)

				PBE-D2* with different S_{rvdw}				PBE-D2* with C_6		
		PBE	PBE-D2	1.10	1.20	1.30	1.40	(M)	(MFX)	exp[a]
CaFCl	a (Å)	3.911 (−0.017)	3.907 (0.013)	3.886 (−0.008)	3.892 (−0.002)	3.904 (0.010)	3.910 (0.016)	3.900 (0.006)	3.903 (0.009)	3.894
	c (Å)	6.865 (0.047)	6.833 (0.015)	6.893 (0.075)	6.841 (0.023)	6.816 (−0.002)	6.794 (−0.024)	6.860 (0.042)	6.835 (0.017)	6.818
	z_X	0.6430 (0.0000)	0.6440 (0.0010)	0.6440 (0.0010)	0.6420 (−0.0010)	0.6420 (−0.0010)	0.6420 (−0.0010)	0.6450 (0.0020)	0.6440 (0.0010)	0.6430
	z_M	0.1940 (−0.0020)	0.1910 (−0.0050)	0.1920 (−0.0040)	0.1940 (−0.0020)	0.1960 (0.0000)	0.1960 (0.0000)	0.1920 (−0.0040)	0.1930 (−0.0030)	0.1960
CaFBr	a (Å)	3.926 (0.043)	4.003 (0.120)	3.932 (0.049)	3.904 (0.021)	3.906 (0.023)	3.913 (0.030)	3.961 (0.078)	3.970 (0.087)	3.883
	c (Å)	8.205 (0.154)	7.385 (−0.666)	7.905 (−0.146)	8.141 (0.090)	8.156 (0.105)	8.095 (0.044)	7.596 (−0.455)	7.534 (−0.517)	8.051
	z_X	0.6710 (0.0010)	0.6517 (−0.0183)	0.6629 (−0.0071)	0.6678 (−0.0022)	0.6677 (−0.0023)	0.6669 (−0.0031)	0.6553 (−0.0147)	0.6545 (−0.0155)	0.6700
	z_M	0.1603 (−0.0097)	0.1710 (0.0010)	0.1638 (−0.0062)	0.1618 (−0.0082)	0.1626 (−0.0074)	0.1631 (−0.0069)	0.1696 (−0.0004)	0.1706 (0.0006)	0.1700
SrFCl	a (Å)	4.130 (0.004)	4.118 (−0.008)	4.101 (−0.025)	4.105 (−0.021)	4.119 (−0.007)	4.116 (−0.010)	4.120 (−0.006)	4.122 (−0.004)	4.126
	c (Å)	6.975 (0.017)	6.929 (−0.029)	6.955 (−0.003)	6.970 (0.012)	6.949 (−0.009)	6.951 (−0.007)	6.930 (−0.028)	6.927 (−0.031)	6.958
	z_X	0.6418 (−0.0011)	0.6428 (−0.0001)	0.6418 (−0.0011)	0.6407 (−0.0022)	0.6410 (−0.0019)	0.6413 (−0.0016)	0.6424 (−0.0005)	0.6423 (−0.0006)	0.6429
	z_M	0.2028 (0.0013)	0.1997 (−0.0018)	0.2017 (0.0002)	0.2040 (0.0025)	0.2049 (0.0034)	0.2043 (0.0028)	0.2015 (0.0000)	0.2014 (−0.0001)	0.2015
SrFBr	a (Å)	4.251 (0.033)	4.271 (0.053)	4.210 (−0.008)	4.218 (0.000)	4.241 (0.023)	4.242 (0.024)	4.244 (0.026)	4.250 (0.032)	4.218
	c (Å)	7.355 (0.018)	7.204 (−0.133)	7.435 (0.098)	7.364 (0.027)	7.292 (−0.045)	7.277 (−0.060)	7.230 (−0.107)	7.276 (−0.061)	7.337
	z_X	0.6469 (−0.0010)	0.6485 (0.0006)	0.6491 (0.0012)	0.6450 (−0.0029)	0.6450 (−0.0029)	0.6455 (−0.0024)	0.6482 (0.0003)	0.6481 (0.0002)	0.6479
	z_M	0.1861 (0.0002)	0.1815 (−0.0044)	0.1825 (−0.0034)	0.1873 (0.0014)	0.1888 (0.0029)	0.1885 (0.0026)	0.1838 (−0.0021)	0.1838 (−0.0021)	0.1859
SrFI	a (Å)	4.258 (0.004)	4.409 (0.155)	4.286 (0.032)	4.245 (−0.009)	4.246 (−0.008)	4.251 (−0.003)	4.356 (0.102)	4.366 (0.112)	4.254
	c (Å)	9.148 (0.299)	7.702 (−1.147)	8.521 (−0.328)	8.966 (0.117)	8.977 (0.128)	8.993 (0.144)	7.974 (−0.875)	7.929 (−0.920)	8.849
	z_X	0.6807 (0.0237)	0.6548 (−0.0022)	0.6672 (0.0102)	0.6749 (0.0179)	0.6745 (0.0175)	0.6769 (0.0199)	0.6574 (0.0004)	0.6571 (0.0001)	0.6570
	z_M	0.1497 (−0.0173)	0.1617 (−0.0053)	0.1557 (−0.0113)	0.1527 (−0.0143)	0.1539 (−0.0131)	0.1521 (−0.0149)	0.1622 (−0.0048)	0.1624 (−0.0046)	0.1670
BaFCl	a (Å)	4.441 (0.047)	4.356 (−0.038)	4.294 (−0.100)	4.378 (−0.016)	4.426 (0.032)	4.391 (−0.003)	4.439 (0.045)	4.444 (0.050)	4.394
	c (Å)	7.311 (0.086)	6.928 (−0.297)	7.145 (−0.080)	7.192 (−0.033)	7.209 (−0.016)	7.278 (0.053)	7.209 (−0.016)	7.209 (−0.016)	7.225
	z_X	0.6462 (−0.0010)	0.6498 (0.0026)	0.6450 (−0.0022)	0.6455 (−0.0017)	0.6466 (−0.0006)	0.6450 (−0.0022)	0.6479 (0.0007)	0.6480 (0.0008)	0.6472
	z_M	0.2061 (0.0012)	0.1940 (−0.0109)	0.2072 (0.0023)	0.2145 (0.0096)	0.2156 (0.0107)	0.2104 (0.0055)	0.2041 (−0.0008)	0.2040 (−0.0009)	0.2049
BaFBr	a (Å)	4.580 (0.072)	4.524 (0.016)	4.402 (−0.106)	4.466 (−0.042)	4.560 (0.052)	4.565 (0.057)	4.586 (0.078)	4.590 (0.082)	4.508
	c (Å)	7.548 (0.107)	7.185 (−0.256)	7.530 (0.089)	7.557 (0.116)	7.408 (−0.033)	7.341 (−0.100)	7.424 (−0.017)	7.417 (−0.024)	7.441
	z_X	0.6497 (0.0000)	0.6513 (0.0016)	0.6450 (−0.0047)	0.6424 (−0.0073)	0.6475 (−0.0022)	0.6447 (−0.0050)	0.6510 (0.0013)	0.6511 (0.0014)	0.6497
	z_M	0.1908 (−0.0003)	0.1730 (−0.0181)	0.1896 (−0.0015)	0.1994 (0.0083)	0.2015 (0.0104)	0.1965 (0.0054)	0.1876 (−0.0035)	0.1875 (−0.0036)	0.1911
BaFI	a (Å)	4.668 (0.014)	4.641 (−0.013)	4.477 (−0.177)	4.543 (−0.111)	4.643 (−0.011)	4.677 (0.023)	4.677 (0.023)	4.679 (0.025)	4.654
	c (Å)	8.053 (0.091)	7.611 (−0.351)	8.326 (0.364)	8.148 (0.186)	7.923 (−0.039)	7.741 (−0.221)	7.902 (−0.060)	7.898 (−0.064)	7.962
	z_X	0.6460 (−0.0062)	0.6448 (−0.0074)	0.6476 (−0.0046)	0.6382 (−0.0140)	0.6405 (−0.0117)	0.6448 (−0.0074)	0.6470 (−0.0052)	0.6465 (−0.0057)	0.6522
	z_M	0.1754 (0.0050)	0.1544 (−0.0160)	0.1668 (−0.0036)	0.1816 (0.0112)	0.1856 (0.0152)	0.1812 (0.0108)	0.1713 (0.0009)	0.1716 (0.0012)	0.1704
PbFCl	a (Å)	4.126 (0.016)	4.103 (−0.007)	4.120 (0.010)	4.100 (−0.010)	4.098 (−0.012)	4.107 (−0.003)	4.102 (−0.008)	4.106 (−0.004)	4.110
	c (Å)	7.307 (0.061)	7.154 (−0.092)	7.198 (−0.048)	7.250 (0.004)	7.284 (0.038)	7.296 (0.050)	7.234 (−0.012)	7.232 (−0.014)	7.246
	z_X	0.6498 (0.0001)	0.6482 (−0.0015)	0.6465 (−0.0032)	0.6461 (−0.0036)	0.6481 (−0.0016)	0.6496 (−0.0001)	0.6500 (0.0003)	0.6500 (0.0003)	0.6497
	z_M	0.2017 (−0.0041)	0.2040 (−0.0018)	0.2072 (0.0014)	0.2055 (−0.0003)	0.2028 (−0.0030)	0.2018 (−0.0040)	0.2015 (−0.0043)	0.2013 (−0.0045)	0.2058
PbFBr	a (Å)	4.182 (−0.010)	4.164 (−0.028)	4.192 (0.000)	4.193 (0.001)	4.186 (−0.006)	4.177 (−0.015)	4.174 (−0.018)	4.183 (−0.009)	4.192
	c (Å)	7.919 (0.319)	7.673 (0.073)	7.683 (0.083)	7.614 (0.014)	7.622 (0.022)	7.734 (0.134)	7.695 (0.095)	7.651 (0.051)	7.600
	z_X	0.6582 (0.0081)	0.6547 (0.0046)	0.6535 (0.0034)	0.6506 (0.0005)	0.6518 (0.0017)	0.6542 (0.0041)	0.6547 (0.0046)	0.6540 (0.0039)	0.6501
	z_M	0.1863 (−0.0064)	0.1889 (−0.0038)	0.1933 (0.0006)	0.1939 (0.0012)	0.1924 (−0.0003)	0.1898 (−0.0029)	0.1880 (−0.0047)	0.1884 (−0.0043)	0.1927
PbFI	a (Å)	4.225 (−0.012)	4.250 (0.013)	4.245 (0.008)	4.198 (−0.039)	4.210 (−0.027)	4.232 (−0.005)	4.263 (0.026)	4.268 (0.031)	4.237
	c (Å)	9.284 (0.484)	8.330 (−0.470)	8.807 (0.007)	9.218 (0.418)	8.828 (0.028)	8.655 (−0.145)	8.344 (−0.456)	8.321 (−0.479)	8.800

https://dx.doi.org/10.1021/acs.jpca.9b10357
J. Phys. Chem. A 2020, 124, 1619−1633

Table 2. continued

	PBE	PBE-D2	PBE-D2* with different S_{rvdw}				PBE-D2* with C_6		
			1.10	1.20	1.30	1.40	(M)	(MFX)	exp[a]
z_X	0.6731 (0.0101)	0.6548 (−0.0082)	0.6638 (0.0008)	0.6691 (0.0061)	0.6603 (−0.0027)	0.6584 (−0.0046)	0.6553 (−0.0077)	0.6548 (−0.0082)	0.6630
z_M	0.1572 (−0.0068)	0.1694 (0.0054)	0.1657 (0.0017)	0.1603 (−0.0037)	0.1655 (0.0015)	0.1674 (0.0034)	0.1686 (0.0046)	0.1689 (0.0049)	0.1640

[a]References 119 and 131−134. The deviation of calculated lattice parameters from experimental values is given in parentheses; a positive value refers to the overestimation and a negative value to the underestimation of the experimental value. PBE-D2* (S_{rvdw}) refers to the modified PBE-D2 functional by increasing the van der Waals radii. PBE-D2*(C_6) corresponds to the modified PBE-D2 functional with substituted coefficients C_6 and van der Waals radii (r_{vdw}) as described in the text.

Following the procedure of Peintinger, Oliveira, and Bredow,[103] we developed the corresponding pob-TZVP basis sets for Sr, Ba, Pb, and I. The valence contraction coefficients were optimized using the Billy program developed by Towler.[107] First, the coefficients were successively optimized by minimizing the energy of the reference systems SrFCl, BaFCl, PbFCl, and CaFI to a convergence of 10^{-8} Hartree using the PBE functional. Then, the optimal coefficients were derived from a third-order polynomial fit. The number of primitive basis functions (s/p/d/f) and their contraction for the def2-TZVP and pob-TZVP basis sets are compared in Table 1 for all atoms of the MFX compounds. The new pob-TZVP basis set information for Sr, Ba, Pb, and I can be found in the Supporting Information.

In the following, Grimme's D2 dispersion scheme[40,41] and its modification derived in this work will be described. The dispersion-corrected total energy is given by

$$E_{\text{DFT-D2}} = E_{\text{DFT}} + E_{\text{disp}} \tag{1}$$

where E_{DFT} is the DFT energy of the system and E_{disp} is the dispersion correction energy which is defined in Grimme's D2 scheme as

$$E_{\text{disp}} = -s_6 \sum_{ij} \frac{C_6^{ij}}{R_{ij}^6} f_{\text{dmp}}(R_{ij}) \tag{2}$$

where s_6 is a global scaling factor that only depends on the functional used, $C_6^{ij} = \sqrt{C_6^i \cdot C_6^j}$ is the dispersion coefficient for each atom pair ij of the molecule. R_{ij} is the interatomic distance between atoms i and j, and $f_{\text{dmp}}(R_{ij})$ is a damping function applied to avoid double counting at short-range.[108] $f_{\text{dmp}}(R_{ij})$ is defined by

$$f_{\text{dmp}}(R_{ij}) = \frac{1}{1 + e^{-d(R_{ij}/S_{\text{rvdw}}R_{\text{vdw}} - 1)}} \tag{3}$$

where d determines the steepness of the damping function, R_{vdw} is the sum of van der Waals radii of the two atoms i and j, and S_{rvdw} is a scaling factor used to modify R_{vdw}. The C_6^i coefficients are calculated from the empirical formula

$$C_6^i = 0.05 N I_i \alpha_i^0 \tag{4}$$

where N has values of 2, 10, 18, 36, and 54 for atoms of first, second, third, fourth, and fifth rows in the periodic table, respectively.[40,41] The first ionization potential I_i and the static dipole polarizability α_i^0 are calculated with the PBE0 functional.[25,109,110]

Inspired by the previous work of Civalleri et al.[73] and Jurecka et al.[10] we modified E_{disp} given in eq 2 for the PBE-D2 functional in two ways: (i) By increasing the scaling factor of the van der Waals radii (S_{rvdw}) by 10−40% in increments of 10, hereafter referred to as PBE-D2*(S_{rvdw} 1.10), PBE-D2*(S_{rvdw} 1.20), PBE-D2*(S_{rvdw} 1.30), and PBE-D2*(S_{rvdw} 1.40); (ii) By replacing the C_6 coefficients and van der Waals radii (PBE-D2*(C_6) either for metal atoms only, hereafter referred to as PBE-D2*(C_6(M)), or for all MFX atoms, hereafter referred to as PBE-D2*(C_6(MFX)) with the C_6 coefficients and van der Waals radii of the noble gas atom with the same number of electrons as the number of core electrons of the metal. For example, the C_6 coefficient and van der Waals radius of Pb were replaced with the ones of Xe. The replacement for metal atoms only was suggested by Sauer et al.[111−113] and Andersson[114,115] assuming that the valence electrons of metals screen dispersion interactions more efficiently than non-metals, making them more short range.

https://dx.doi.org/10.1021/acs.jpca.9b10357
J. Phys. Chem. A 2020, 124, 1619−1633

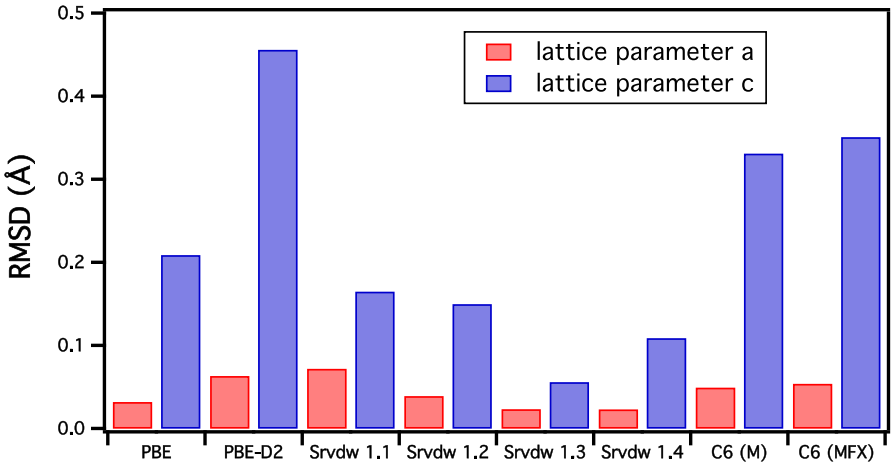

Figure 2. Root-mean-square deviations (RMSDs) of lattice parameters *a* and *c* obtained with PBE, PBE-D2, PBE-D2*(S_{rvdw} 1.10), PBE-D2*(S_{rvdw} 1.20), PBE-D2*(S_{rvdw} 1.30), PBE-D2*(S_{rvdw} 1.40), PBE-D2*(C_6(M)), and PBE-D2*(C_6(MFX)) from experimental values, averaged over all 11 MFX compounds.

All aforementioned calculations with Gaussian-type basis sets were performed with the Crystal14 package.[116] Geometry optimizations used the Monkhorst−Pack[117] grid of 10 × 10 × 8 in combination with the convergence accuracy of 10^{-7} for the Coulomb and exchange integrals. Harmonic vibrational frequencies were evaluated at the center of the Brillouin zone (Γ point). All calculations were performed for the tetragonal Matlockite structure ($P4/nmm$, D_{4h}^7, No. 129),[118,119] which is fully described by the lattice parameters *a* and *c*, and by the fractional coordinates z_M and z_X. The metal, fluoride, and halogen atoms were located on the Wyckoff sites 2c (1/4, 1/4, z_M), 2a, (3/4, 1/4, 0), and 2_c (1/4, 1/4, z_X), respectively.

To further assess the quality of the modified functional, additional calculations with other currently used dispersion-corrected functionals were performed for SrFCl, SrFI, and PbFI compounds. SrFCl was chosen as a representative compound for which PBE and PBE-D2 describe the lattice parameters *a* and *c* reasonably well. SrFI and PbFI were chosen as two representative compounds where both PBE and PBE-D2 fail to reproduce the lattice parameter *c*. The functionals tested were the dispersion-corrected PBE-D3,[42] PBE-TS,[44] and PBE-XDM[45] functionals, the modified B3LYP-D2* functional of Civalleri and co-workers,[73] the semilocal dispersion-corrected M06-2X functional,[27] and the range-separated ωB97X[34,64] and HSE06 functionals.[25,61] PBE-D3, B3LYP-D2*, M06-2X, ωB97X, and HSE06 calculations were performed with the pob-TZVP basis set[103] using the Crystal17 program package.[120] PBE-TS[44] calculations were performed with projector-augemented plane-wave (PAW) potentials[121,122] and the energy cutoff of 400 eV using the VASP program package version 5.4.4.[123−127] The PBE-XDM[45] calculations were performed with PAW potentials[121,122] along with the wave function and density cutoffs of 110 and 120 Ry using the Quantum Espresso program package version 6.4.1.[128,129]

RESULTS AND DISCUSSION

In the following, the performance of the six modified PBE-D2* functionals PBE-D2*(S_{rvdw} 1.10), PBE-D2*(S_{rvdw} 1.20), PBE-D2*(S_{rvdw} 1.30), PBE-D2*(S_{rvdw} 1.40), PBE-D2*(C_6(M), and PBE-D2*(C_6(MFX) is discussed, with regard to reproducing the experimental crystal structure parameters, interatomic distances, and vibrational frequencies. We will also assess their performance in comparison with other currently used DFT functionals.

Crystal Structure Parameters. Table 2 summarizes the calculated lattice parameters *a* and *c* and fractional coordinates z_M and z_X and their derivation from the experimental values (given in parentheses) for the 11 MFX compounds investigated in this work, using the PBE and PBE-D2 functionals as well as our six modified PBE-D2* functionals. In Figure 2 the root-mean-square deviations (RMSD) of lattice parameters *a* and *c* obtained with PBE, PBE-D2, PBE-D2*(S_{rvdw} 1.10), PBE-D2*(S_{rvdw} 1.20), PBE-D2*(S_{rvdw} 1.30), PBE-D2*(S_{rvdw} 1.40), PBE-D2*(C_6(M)), and PBE-D2*(C_6(MFX)) from the experimental values for all 11 MFX compounds are shown. In general, the lattice parameters *a* and *c* along with the volume increase with increasing ionic radius, e.g., for the PbFX compounds the experimental lattice parameter *c* increases from 7.246 to 8.800 Å by replacing Cl with I. As shown in Table 2, the increase of the lattice parameter *c* is larger than the increase of the lattice parameter *a*.

All functionals including PBE reproduce the lattice parameter *a* reasonably well with RMSDs ranging from 0.02 to 0.07 Å, averaged over the entire set of studied compounds (see Figure 2 and also Supporting Information Figure S1). This result suggests that dispersion correction does not play a significant role for the calculation of lattice parameter *a*. The inclusion of Grimme's D2 empirical dispersion correction, (PBD-D2), slightly increases the RMSD to 0.06 Å compared to an RMSD of 0.03 Å for PBE. The modified PBE-D2*(C_6(M)) and PBE-D2*(C_6(MFX)) functionals also have a slightly increased lattice parameter *a* with an RMSD value of 0.05 Å for both functionals. An increase of the van der Waals radii by 10% leads to a slightly increased RMSD value (D2*(S_{rvdw} 1.10), RMSD = 0.07 Å), whereas the smallest RMSD of 0.02 Å is found for the 30 and 40% increased van der Waals radii, PBE-D2*(S_{rvdw} 1.30) and PBE-D2*(S_{rvdw} 1.40), respectively.

This overall good performance is no longer found for lattice parameter *c*. Due to the presence of a double halide layer along the *c* axis, $F^-−M^{2+}−X^-\cdots X'^-−M'^{2+}−F'^-$ with weak X···X′, M′−X, and M−X′ interactions, the description of lattice parameter *c* is more challenging. PBE tends to overestimate the lattice parameter *c* due to missing dispersion interactions, as previously reported by D'Anna and co-workers.[95] For CaFCl and SrFCl, PBE results are still reasonable; however, as the

https://dx.doi.org/10.1021/acs.jpca.9b10357
J. Phys. Chem. A 2020, 124, 1619−1633

atomic radius of atom X increases, PBE results significantly deviate from the experimental values, as shown in Table 2.

However, inclusion of empirical dispersion correction via the PBE-D2 functional leads in most cases to a significant underestimation of lattice parameter c with an RMSD value of 0.46 Å, averaged over the entire set of studied compounds, and a maximum deviation of 1.147 Å for SrFI, as shown in Table 2. PBE-D2 obviously overemphasizes the attractive forces between the two halide layers (see also further discussion in the subsection Interatomic Distances). This is most likely due to the fact that the original D2 correction was calibrated for molecular complexes, leading to an unbalanced description of the dispersion in crystalline systems, as pointed out by Civalleri and co-workers.[73]

Although the PBE-D2*(C_6) functionals contain only ca. 30% of the original D2 dispersion, the improvement with regard to the D2 correction is only marginal as reflected by RMSD values of 0.33 and 0.35 Å for PBE-D2*(C_6(M)) and PBE-D2*-(C_6(MFX)) respectively, averaged over the entire set of studied compounds. However, increasing the van der Waals radii by 10% leads already to a significant improvement (RMSD of PBE-D2 = 0.46 Å compared to RMSD of PBE-D2*(S_{rvdw} 1.10) = 0.17 Å). The optimum value is found for an increase of 30% (RMSD of PBE-D2*(S_{rvdw} 1.30) = 0.06 Å). As pointed out by Civalleri and co-workers, the increase of the van der Waals radii as they enter the damping function in eq 3 allows us to switch on the dispersion term only at a longer distance, thus decreasing the overall dispersion contribution.[73] The best results were obtained for our modified PBE-D2*(S_{rvdw} 1.30) functional reproducing the lattice parameters a and c with maximum deviations of 0.03 and 0.13 Å, respectively; see Table 2.

We compared the performance of the PBE-D2*(S_{rvdw} 1.30) functional with that of a number of popular dispersion correction schemes: C_6-based corrections PBE-D3, PBE-TS, PBE-XDM, and B3LYP-D2*; dispersion-corrected semilocal functional M06-2X; and range-separated functionals ωB97X and HSE06 for the SrFCl, SrFI, and PbFI compounds, shown in Figure 3. Again, these functionals lead to a reasonable description of lattice parameter a with deviations of 0.05, 0.08, and 0.07 Å for PBE-TS, PBE-XDM, and M06-2X, respectively. The calculated lattice parameter c obtained with PBE-D3, PBE-TS, PBE-XDM, B3LYP-D2*, M06-2X, ωB97X, and HSE06 significantly deviates from experimental values: PBE, PBE-TS, and B3LYP-D2* overestimate the lattice parameter c with maximum deviations of 0.48, 0.87, and 0.76 Å, respectively, while PBE-D2 and M06-2X underestimate with maximum deviations of −1.04 and −0.96 Å, respectively. In summary, the modified PBE-D2*(S_{rvdw} 1.30) functional outperforms PBE, PBE-D2, and the other five modified PBE-D2* functionals as well as the other dispersion-corrected functionals tested in this work (see Figure 2 and Figure S1 of the Supporting Information). It is noteworthy that the experimental lattice parameters were obtained at room temperature. Comparison with low temperature data at 100 K shows that the thermal effects are relatively small by 0.014 and 0.008 Å for lattice parameters a and c, respectively.[130]

Interatomic Distances. To further elucidate the performance of the six modified functionals in comparison with PBE and PBE-D2, we analyzed the reproducibility of the experimental interatomic distances. The calculated M−F, M−X, M−X′, and X···X′ interatomic distances and their deviations from the experimental values (given in parentheses) for the 11 MFX compounds investigated in this work, calculated with the PBE and PBE-D2 functionals as well as with our six modified PBE-D2*

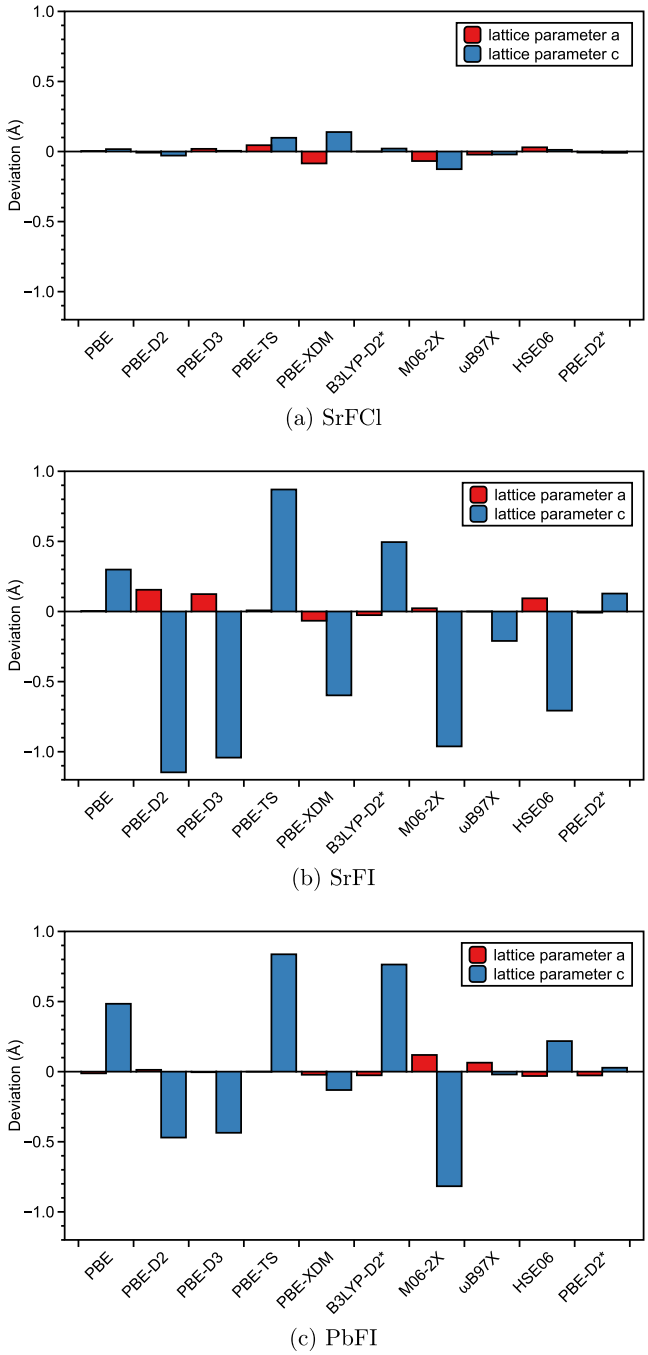

Figure 3. Deviation of lattice parameters a and c from experimental data for (a) SrFCl, (b) SrFI, and (c) PbFI obtained with PBE, PBE-D2, PBE-D3, PBE-TS, PBE-XDM, B3LYP-D2*, M06-2X, ωB97X, HSE06, and PBE-D2*. PBE-D2* refers to the modified PBE-D2*(S_{rvdw} 1.30)) functional.

functionals is summarized in Table S4 of Supporting Information. In Figure 4, the correlation between calculated and experimental interatomic distances are plotted. In the ideal case, i.e., 100% reproduction of experimental values, all points would lie on the black solid line with an r^2 value of 1; i.e., the r^2 values in Figure 4 provide a direct measure of quality of the functional used. The best overall agreement between experimental and calculated distances is achieved for the M−X distance, with r^2 values ranging from 0.96 for PBE-D2 to 0.99 for the modified PBE-D2*(S_{rvdw} 1.30) functional, as shown in Figure 4a. The r^2 values for the M−F distances are slightly smaller with PBE, PBE-D2*(S_{rvdw} 1.30),

https://dx.doi.org/10.1021/acs.jpca.9b10357
J. Phys. Chem. A 2020, 124, 1619−1633

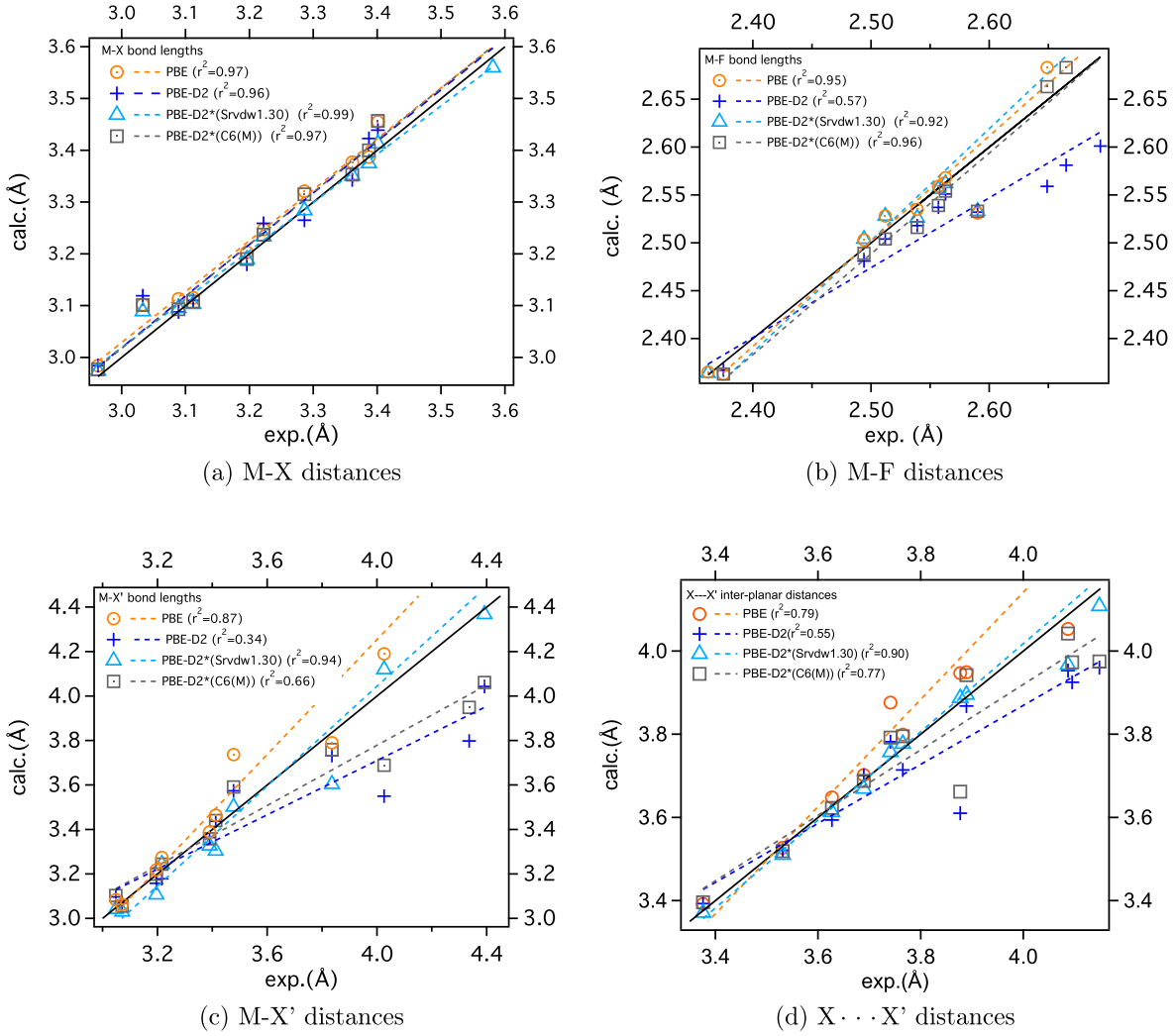

Figure 4. Calculated and experimental M−F, M−X, M−X′, and X···X′ interatomic distances. The M−X′ and X···X′ distances are along the *c*-axis. The solid black line denotes 100% agreement between calculated and experimental values. The r^2 values in the legend reflect the deviation from the ideal line. The orange circle, light blue triangle, dark blue cross, and gray square correspond to the values obtained from PBE, PBE-D2, and PBE-D2*(S_{rvdw} 1.30), and PBE-D2*(C_6(M)), respectively.

Table 3. Calculated Harmonic and Available Experimental Vibrational Frequencies of MFX (M = Ca, Sr, Ba, Pb and X = Cl, Br, I)

				PBE-D2* with different S_{rdw}				C_6		
	mode	PBE	PBE-D2	1.10	1.20	1.30	1.40	M	MFX	exp[a]
CaFCl	$1e_g$	168	172	168	171	170	168	172	172	156
	$1a_{1g}$	202	213	199	208	208	210	208	209	192
	$2e_g$	204	209	203	209	209	207	206	207	209
	$2a_{1g}$	278	279	281	283	278	276	280	279	265
	b_g	262	275	271	265	262	263	274	272	252
	$3e_g$	347	359	359	351	348	347	361	356	336
SrFCl	$1e_g$	115	116	118	119	115	115	117	116	107
	$1a_{1g}$	173	169	175	182	178	177	173	173	155
	$2e_g$	180	187	183	184	184	185	185	183	169
	$2a_{1g}$	214	217	216	214	214	214	217	214	198
	b_g	251	262	261	250	248	250	260	257	246
	$3e_g$	312	319	326	314	311	313	318	315	302
BaFCl	$1e_g$	79	84	95	91	75	77	80	80	89
	$1a_{1g}$	131	139	156	153	140	140	132	131	125
	$2e_g$	141	162	169	157	145	150	140	141	142
	$2a_{1g}$	165	185	196	192	184	175	165	164	161
	b_g	215	273	254	214	202	215	224	222	212
	$3e_g$	253	309	297	260	246	257	257	256	247

https://dx.doi.org/10.1021/acs.jpca.9b10357
J. Phys. Chem. A 2020, 124, 1619−1633

Table 3. continued

				PBE-D2* with different S_{rdw}				C_6		
	mode	PBE	PBE-D2	1.10	1.20	1.30	1.40	M	MFX	exp[a]
BaFBr	$1e_g$	70	82	87	78	65	68	73	73	76
	$1a_{1g}$	95	118	114	115	106	104	98	98	105
	$2e_g$	98	128	119	116	113	117	101	101	109
	$2a_{1g}$	123	131	149	145	121	124	123	122	119
	b_g	211	253	248	208	198	211	219	218	215
	$3e_g$	234	291	279	246	227	236	239	238	240
BaFI	$1e_g$	64	83	72	72	62	63	71	71	70
	$1a_{1g}$	76	117	91	88	87	89	89	89	79
	$2e_g$	101	125	119	118	105	104	105	105	105
	$2a_{1g}$	118	133	149	144	119	114	118	118	113
	b_g	205	238	243	206	193	207	213	211	203
	$3e_g$	227	281	274	242	222	226	232	231	218
PbFCl	$1e_g$	45	56	45	45	48	48	51	50	43.5
	$1a_{1g}$	104	116	111	108	109	107	109	109	105.5
	$2e_g$	125	137	137	133	131	129	132	128	134
	$2a_{1g}$	162	172	174	166	166	165	168	165	164.5
	b_g	209	221	206	205	211	213	222	219	226.5
	$3e_g$	249	257	255	250	253	254	257	253	241
PbFBr	$1e_g$	42	53	41	39	43	45	46	46	39
	$1a_{1g}$	81	100	93	88	90	88	89	88	89
	$2e_g$	79	91	90	89	90	86	96	95	95
	$2a_{1g}$	117	123	118	115	117	118	121	119	116.5
	b_g	226	242	226	223	228	230	240	236	224.5
PbFI	$1e_g$	20	42	21	20	27	28	32	31	36
	$2e_g$	61	79	64	62	69	70	79	79	61
	$1a_{1g}$	75	98	85	75	79	60	91	91	67
	$2a_{1g}$	110	117	111	110	112	111	112	112	105.5
	b_g	201	216	207	200	205	207	197	195	206
	$3e_g$	200	201	208	206	203	204	216	214	

[a]Experimental frequencies of CaFCl, SrFCl, BaFBr, and BaFI from ref 138, BaFCl from ref 139, PbFCl and PbFBr from ref 140, and PbFI from ref 141. The LO-TO splitting of infrared active modes of BaFCl can be found in Table S3, Supporting Information.

and PBE-D2*(C_6(M)), in line with the finding that the description of M−F bonds in crystals is more difficult than that for higher halogen homologues.[1,96] PBE-D2 falls short with an r^2 value of 0.57, substantially underestimating the M−F distance, obviously due to overemphasizing metal−fluoride bonding in the solid state. More critical are the M−X′ and X···X′ interactions along the *c* lattice axis, shown in Figure 4c,d. In both cases, results obtained from the PBE functional overestimate the M−X′ and X···X′ interatomic distances along the *c*-axis due to the missing dispersion, while the inclusion of empirical dispersion corrections via PBE-D2 leads to too short distances, resulting from an overcorrection of dispersion effects. Scaling of the van der Waals radii (S_{rvdw}) allows us to fine-tune the attractive forces describing the M−X′ and X···X′ interactions along the *c* axis. The modified PBE-D2*(S_{rvdw} 1.30) functional leads in both cases to best the agreement with the experimental results as reflected by r^2 values of 0.94 and 0.90, respectively, reflecting that PBE-D2*(S_{rvdw} 1.30) provides a balanced description of the M−F, M−X, M−X′, and X···X′ interatomic distances.

Vibrational Frequencies. MFX has two formula units per unit cell. At the center of the Brillouin zone, MFX has 12 vibrational modes that transform into $2 \times a_{1g}$, $1 \times b_{1g}$, $3 \times e_g$, $3 \times a_{2u}$, and $3 \times e_u$, where e_g and e_u are doubly degenerate modes. The a_{1g}, b_{1g}, and e_g modes are Raman active, while the a_{2u} and e_u modes are IR active, and the a_{2u} and e_u modes are acoustic modes. The $3 \times e_g$ vibrational modes describe the motion along

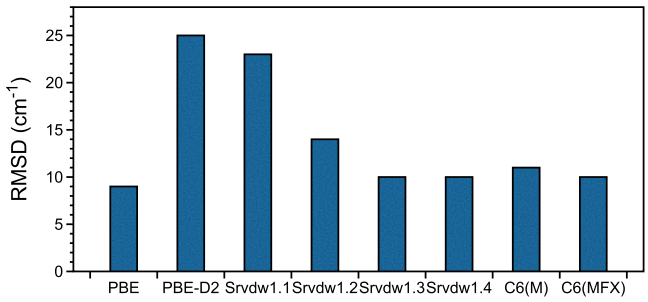

Figure 5. Root-mean-square deviations (RMSDs) of the vibrational frequencies obtained from PBE, PBE-D2, PBE-D2*(S_{rvdw} 1.10), PBE-D2*(S_{rvdw} 1.20), PBE-D2*(S_{rvdw} 1.30), PBE-D2*(S_{rvdw} 1.40), PBE-D2*(C_6(M)), and PBE-D2*(C_6(MFX)) in cm^{-1} from the experimental values, averaged over all 11 MFX compounds.

lattice parameter *a* whereas the $2 \times a_{1g}$ modes and the b_{1g} mode are related to lattice parameter *c* (see Supporting Information). The $1e_g$ refers to the shear mode characterized by the displacement of the X^- planes in opposite directions (see Figure S2, Supporting Information). The $1a_{1g}$ mode corresponds to the breathing mode of the double anionic X^- layer with the cation M^{2+} planes moving in the same direction. The $2e_g$ mode represents M−X stretching. The $2a_{1g}$ mode is associated with the analogous to the $1a_{1g}$ mode, except the cation M^{2+} layers move in the opposite direction. The b_{1g} and $3e_g$ modes are associated with the motions of the fluoride ions.

https://dx.doi.org/10.1021/acs.jpca.9b10357
J. Phys. Chem. A 2020, 124, 1619−1633

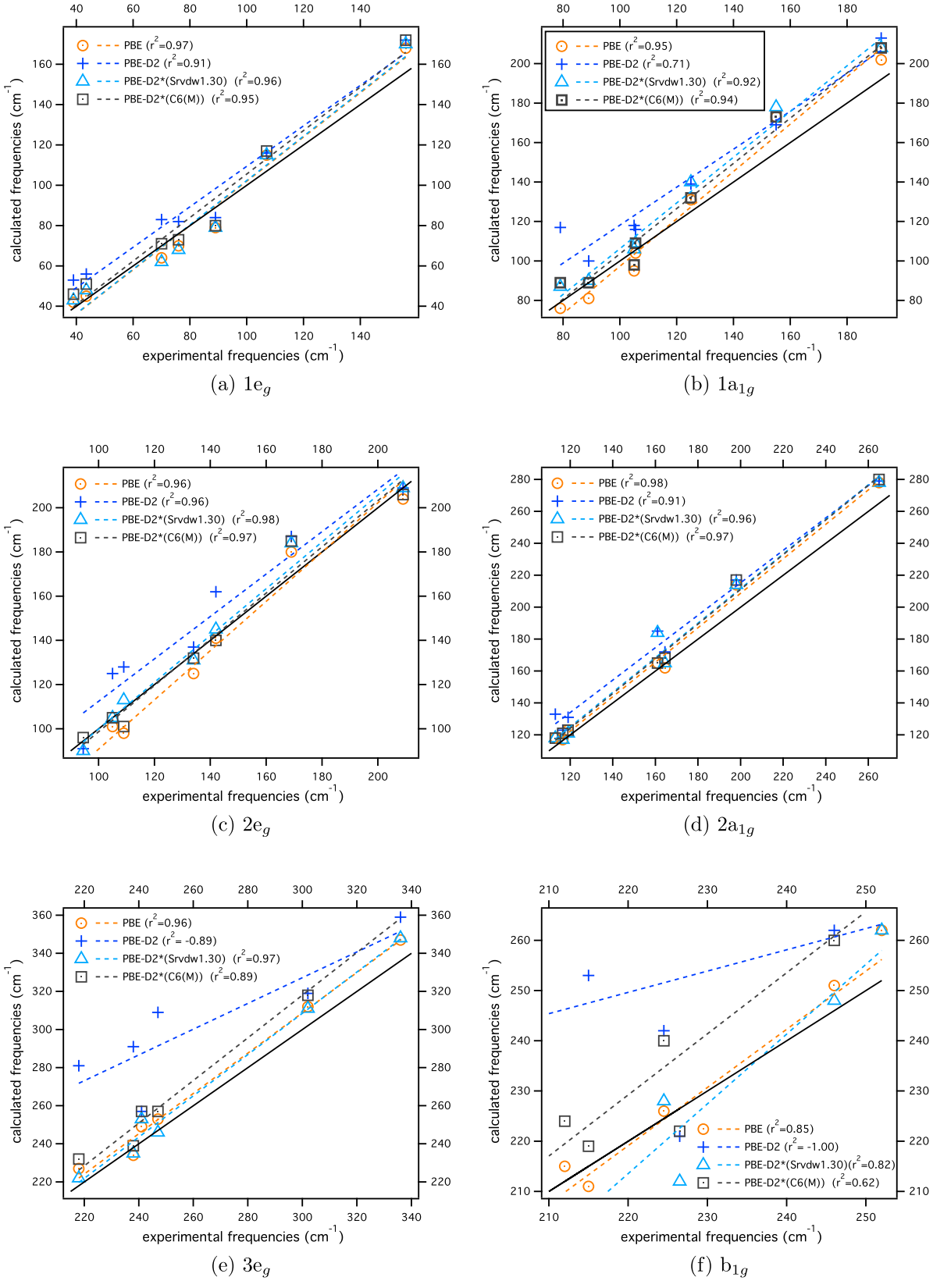

Figure 6. Correlation between calculated and experimental frequencies for $1e_g$, $1a_{1g}$, $2e_g$, $2a_{1g}$, $3e_g$, b_{1g}. The solid black line denotes 100% agreement between calculated and experimental values. The r^2 values in the legend reflect the deviation from the ideal line. The orange circle, light blue triangle, dark blue cross, and gray square correspond to the values obtained from PBE, PBE-D2, and PBE-D2*(S_{rvdw} 1.30), and PBE-D2*(C_6(M)), respectively.

Table 3 compares the calculated harmonic frequencies obtained with the PBE, PBE-D2, PBE-D2*(S_{rvdw} = 1.10), PBE-D2*(S_{rvdw} = 1.20), PBE-D2*(S_{rvdw} = 1.30), PBE-D2*(S_{rvdw} 1.40), PBE-D2*($C_6(M)$), and PBE-D2*(C_6(MFX)) with the experimental values, i.e. excluding anharmonic effects, which may play a larger role in the case of heavier atoms. It also should be noted

https://dx.doi.org/10.1021/acs.jpca.9b10357
J. Phys. Chem. A 2020, 124, 1619−1633

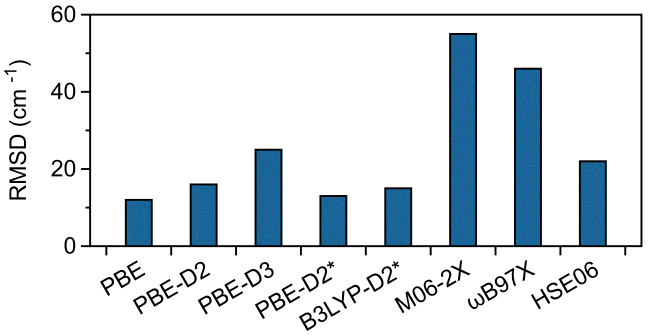

Figure 7. Root-mean-square deviations (RMSDs) of the vibrational harmonic frequencies for SrFCl obtained from PBE, PBE-D2, PBE-D3, PBE-D2*, B3LYP-D2*, M06-2X, ωB97X, and HSE06 from the experimental values.

Table 4. Calculated Equilibrium Volume at Zero Pressure (V_0), Bulk Modulus (B_0) and Its Derivative (B_0'), and Elastic Constant (C_{33})

		V_0 (Å^3)	B_0 (GPa)	B_0'	C_{33} (GPa)
SrFCl	PBE	119.03	64.35	4.32	92.67
	PBE-D2	117.51	64.36	3.89	88.23
	PBE-D2*(S_{rvdw} 1.30)	117.95	65.33	4.14	96.28
	PBE-D2*(C_6(M))	117.64	64.57	4.42	92.23
	exp[a]	118.45	61.00	5.00	
BaFI	PBE	175.58	30.86	9.68	39.25
	PBE-D2	163.87	54.66	2.80	97.34
	PBE-D2*(S_{rvdw} 1.30)	170.64	39.79	5.17	46.71
	PBE-D2*(C_6(M))	172.78	40.92	4.44	51.92
	exp[b]	172.45	36.00	6.00	

[a]Reference 142. [b]Reference 143.

that the experimental frequencies are shifted by about 5−10 cm^{-1} over a temperature range of 10−300 K.[135] In Figure 5, the overall RMSDs of the calculated vibrational frequencies from the experimental values averaged over all 11 MFX compounds are shown. As reflected by the data in Table 3, larger deviations are found for the heavier halogens. The overall RMSDs of PBE, PBE-D2, PBE-D2*(S_{rvdw} 1.10), PBE-D2*(S_{rvdw} 1.20), PBE-D2*(S_{rvdw} 1.30), PBE-D2*(S_{rvdw} 1.40), PBE-D2*(C_6(M)), and PBE-D2*(C_6(MFX)) are 9, 25, 23, 14, 10, 10, 11, 10 cm^{-1}, respectively, with the largest deviation from the experimental values found for the PBE-D2 functional. The PBE, PBE-D2*(S_{rvdw} 1.30), PBE-D2*(S_{rvdw} 1.40), PBE-D2*(C_6(M)), and PBE-D2*-(C_6(MFX)) results are comparable with deviations of 10−15 cm^{-1}.

Figure 6 shows the correlation between calculated harmonic and experimental frequencies for the 11 MFX compounds obtained with PBE, PBE-D2, PBE-D2*(S_{rvdw} 1.30), and PBE-D2*(C_6(M)) for the individual modes $1e_g$, $2e_g$, and $3e_g$, Figures 6a,c,e, with an overall motion along the lattice parameter a, and for the individual modes $1a_{1g}$, $2a_{1g}$, and b_{1g}, Figures 6b,d,e, being related to the motion along the lattice parameter c. In contrast to the interatomic distances, the results shown in Table 3 and Figure 6 do not reveal that the reproduction of the experimental frequencies corresponding to the motion along the lattice parameter c is particularly poor. Reasonable frequencies for all eight functionals including PBE are obtained for the $1e_g$ and $2e_g$ modes (related to lattice parameter a) with r^2 values in the range 0.96−0.98. The same holds for the $2a_{1g}$ mode (related to lattice parameter c). In the case of the $1a_{1g}$ mode, PBE-D2 results fall short with an r^2 value of 0.71 and it totally fails in the case of the $3e_g$ and b_{1g} modes with r^2 values of −0.89 and −1.00. This is in line with the reported failure of LDA and GGA functionals to reproduce the b_{1g} symmetrical frequency of the BaFCl compound.[95] The overall accuracy of the modified PBE-D2*(S_{rvdw} 1.30), PBE-D2*(S_{rvdw} 1.40), PBE-D2*(C_6(M)), and PBE-D2*(C_6(MFX)) functionals with RMSD values of 9, 10, 10, 11, and 10 cm^{-1}, respectively matches the error bars of the experimental frequencies.[136,137]

We compared the performance of PBE-D2*(S_{rvdw} 1.30) with that of a number of popular dispersion correction schemes: C_6-based corrections PBE-D2, PBE-D3, and B3LYP-D2*; dispersion-corrected semilocal functional M06-2X; and range-separated functionals ωB97X and HSE06 for the SrFCl, shown in Figure 7. PBE-D3, M06-2X, ωB97X, and HSE06 deviate significantly from the experimental values: RMSD of PBE-D3, 25 cm^{-1}; RMSD of M06-2X, 55 cm^{-1}; RMSD of ωB97X, 46 cm^{-1}; RMSD of HSE06, 22 cm^{-1}. PBE-D2 and B3LYP-D2* perform better with RMSDs of 16 and 15 cm^{-1}, respectively. Overall, PBE (RMSD of 12 cm^{-1}) and PBE-D2*(S_{rvdw} 1.30) (RMSD of 13 cm^{-1}) outperform PBE-D2, PBE-D3, B3LYP-D2*, M06-2X, ωB97X, and HSE06 (see Figure 7 and Table S2, Supporting Information).

Mechanical Properties. To further evaluate the performance of the modified functional in comparison with PBE and PBE-D2, we examined the reproducibility of experimentally determined mechanical properties. Table 4 summarizes the calculated equilibrium volume at zero pressure (V_0), bulk modulus (B_0) and its derivative (B_0'), and elastic constant (C_{33}) for two representative compounds. In Figure 8, the calculated pressure versus volume curve and the fitted curve obtained from the Vinet equation of state are plotted. In the case of SrFCl, where PBE, PBE-D2, and the modified functional describe the lattice parameters reasonably well, all methods (PBE, PBE-D2, PBE-D2*(S_{rvdw} 1.30), and PBE-D2*(C6(M)) give reasonable results for V_0, B_0, and B_0', leading to similar curvatures. On the contrary, in the case of BaFI, where PBE and PBE-D2 fail to reproduce the lattice parameter c, PBE and PBE-D2 also fail to reproduce the experimental values. PBE-D2*(S_{rvdw} 1.30) and PBE-D2*(C6(M)) give accurate results, where PBE-D2*(S_{rvdw} 1.30) performs slightly better than PBE-D2*(C_6(M)). In summary, the modified PBE-D2*(S_{rvdw} 1.30) functional leads in both cases to the best agreement with the experimental values.

CONCLUSIONS

We investigated how standard and dispersion-corrected functionals reproduce lattice parameters, interatomic distances, and vibrational frequencies of inorganic layered MFX compounds. As a test set we used 11 different MFX compounds (M = M′ = Ca, Ba, Sr, Pb and X = X′ = Cl, Br, I) crystallized in the tetragonal Matlockite structure for which experimental data are available. This family of crystals presents a stacking of double halide layers, $F^--M^{2+}-X^-\cdots X'^-M'^{2+}-F'^-$, along the c axis. Using standard DFT functionals, such as PBE, the description of this double halide layer is not satisfactory, the lattice parameter c tends to be systematically overestimated, suggesting the importance of dispersion interactions. However, the inclusion of dispersion correction, e.g., via the popular Grimme D2 correction scheme does not lead to an improvement over the PBE results but tends to deteriorate the description of the MFX compounds due to an unbalanced coverage of dispersion needed for the description of the weak interactions in these crystals. Good agreement between calculations and experiments can be achieved by systematically modifying the parameters of the original D2 dispersion correction

https://dx.doi.org/10.1021/acs.jpca.9b10357
J. Phys. Chem. A 2020, 124, 1619−1633

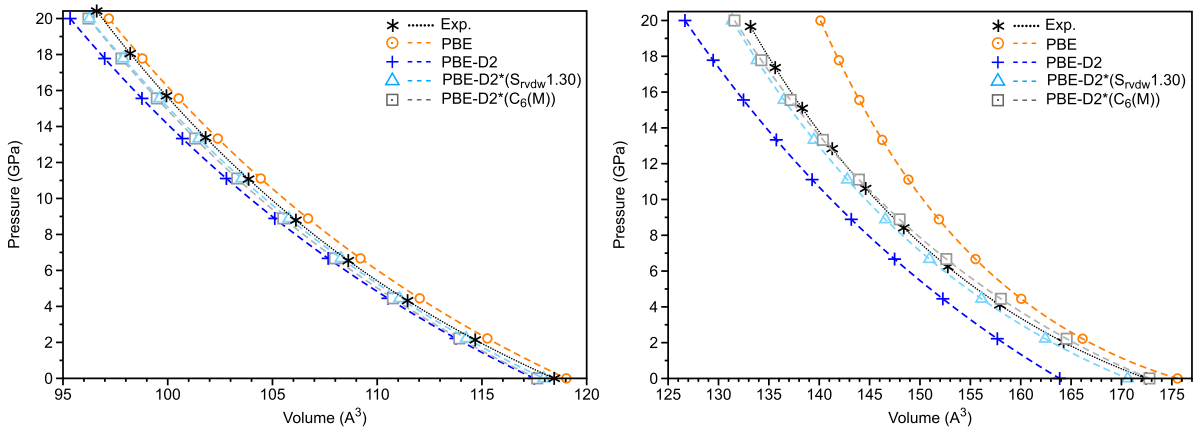

Figure 8. Calculated pressure−volume of (a) SrFCl and (b) BaFI and fitted using the Vinet equation of state.

scheme. In particular, increasing the van der Waals radii by 30% (PBE-D2*(S_{rvdw} 1.30)) allows us to fine-tune the description of the weak interactions between the halide layers along the lattice axis *c*, leading to an improved description of structural, vibrational, and mechanical properties. As revealed by our study, the modified PBE-D2*(S_{rvdw} 1.30) functional also outperforms other C_6-based scheme such as PBE-D3, PBE-TS, PBE-XDM, B3LYP-D2*, dispersion-corrected semilocal functionals such as M06-2X, and range-separated hybrid functionals such as ωB97X, and HSE06 tested in this work.

The correct description of the lattice parameters, in particular that of the lattice parameter *c*, is important for the prediction of mechanical and elastic properties as well as phase transitions taking place in these MFX inorganic layered compounds. Work is in process applying the new PBE-D2*(S_{rvdw} 1.30) modification to other compounds with double halogen layers, to elucidate the nature of the X···X′ interactions in double halide layers and to determine their intrinsic strength with the Local Vibrational Mode Analysis.[74,144−147]

■ ASSOCIATED CONTENT

Supporting Information

The Supporting Information is available free of charge at https://pubs.acs.org/doi/10.1021/acs.jpca.9b10357.

Calculated lattice parameters for SrFCl, SrFI, and PbFI obtained from PBE-D3, PBE-TS, B3LYP-D*, M06-2X, ωB97X, HSE06; calculated vibrational frequencies of SrFCl obtained from PBE, B3LYP, M06-2X, ωB97X, HSE06; calculated and experimental LO-TO splitting; calculated and experimental bond distances; calculated and experimental lattice parameters; calculated LO-TO splitting of infrared active modes of BaFCl; RMSD deviations of cell parameters and MAD of lattice parameters; pob-TZVP basis sets for Sr, Ba, Pb, and I; eigenvector displacement of $1e_g$, $1a_{1g}$, $2e_g$, $2a_{1g}$, b_g, $3e_g$ modes; calculated total energy vs volume and vs lattice parameter (PDF)

■ AUTHOR INFORMATION

Corresponding Author

Elfi Kraka − *Computational and Theoretical Chemistry Group (CATCO), Department of Chemistry, Southern Methodist University, Dallas, Texas 75275-0314, United States;* orcid.org/0000-0002-9658-5626; Email: ekraka@gmail.com

Authors

Daniel Sethio − *Computational and Theoretical Chemistry Group (CATCO), Department of Chemistry, Southern Methodist University, Dallas, Texas 75275-0314, United States;* orcid.org/0000-0002-8075-1482

João B. L. Martins − *Institute of Chemistry, University of Brasilia, Brasilia, DF 70910-900, Brazil;* orcid.org/0000-0001-8677-3239

Latévi Max Lawson Daku − *Department of Physical Chemistry, University of Geneva, CH-1211 Geneva 4, Switzerland;* orcid.org/0000-0003-1305-6807

Hans Hagemann − *Department of Physical Chemistry, University of Geneva, CH-1211 Geneva 4, Switzerland;* orcid.org/0000-0002-7183-8543

Complete contact information is available at: https://pubs.acs.org/10.1021/acs.jpca.9b10357

Notes

The authors declare no competing financial interest.

■ ACKNOWLEDGMENTS

This work was supported by the National Science Foundation (Grant CHE 1464906), the Swiss National Science Foundation (project 200021-169033), and the Brazilian National Council for Scientific and Technological Development (CNPq 310071/2018-6) and the Foundation for Research of Federal District/Brazil (FAPDF 0193.001642/2017). The authors thank Southern Methodist University and the University of Geneva for providing excellence computational resources. The authors thank Dr. Céline Besnard (University of Geneva) for providing the low temperature crystal structure.

■ REFERENCES

(1) Stohr, M.; Van Voorhis, T.; Tkatchenko, A. Theory and Practice of Modeling van der Waals Interactions in Electronic-Structure Calculations. *Chem. Soc. Rev.* **2019**, *48*, 4118−4154.

(2) Dubecký, M.; Mitas, L.; Jurečka, P. Noncovalent Interactions by Quantum Monte Carlo. *Chem. Rev.* **2016**, *116*, 5188−5215.

(3) Ambrosetti, A.; Ferri, N.; DiStasio, R. A., Jr.; Tkatchenko, A. Wavelike Charge Density Fluctuations and van der Waals Interactions at the Nanoscale. *Science* **2016**, *351*, 1171.

(4) Stone, A. *The Theory of Intermolecular Forces*; Oxford University Press: Oxford, 2013.

(5) Černý, J.; Hobza, P. Non-Covalent Interactions in Biomacromolecules. *Phys. Chem. Chem. Phys.* **2007**, *9*, 5291.

(6) Fabrizio, A.; Grisafi, A.; Meyer, B.; Ceriotti, M.; Corminboeuf, C. Electron Density Learning of Non-Covalent Systems. *Chem. Sci.* **2019**, *10*, 9424−9432.
(7) Pastorczak, E.; Corminboeuf, C. Perspective: Found in Translation: Quantum Chemical Tools for Grasping Non-Covalent Interactions. *J. Chem. Phys.* **2017**, *146*, 120901.
(8) Granatier, J.; Pitoňák, M.; Hobza, P. Accuracy of Several Wave Function and Density Functional Theory Methods for Description of Noncovalent Interaction of Saturated and Unsaturated Hydrocarbon Dimers. *J. Chem. Theory Comput.* **2012**, *8*, 2282−2292.
(9) Vondrášek, J.; Bendová, L.; Klusák, V.; Hobza, P. Unexpectedly Strong Energy Stabilization Inside the Hydrophobic Core of Small Protein Rubredoxin Mediated by Aromatic Residues: Correlated Ab Initio Quantum Chemical Calculations. *J. Am. Chem. Soc.* **2005**, *127*, 2615−2619.
(10) Jurečka, P.; Černý, J.; Hobza, P.; Salahub, D. R. Density Functional Theory Augmented with an Empirical Dispersion Term. Interaction Energies and Geometries of 80 Noncovalent Complexes Compared with Ab Initio Quantum Mechanics Calculations. *J. Comput. Chem.* **2007**, *28*, 555−569.
(11) Christensen, A. S.; Kubař, T.; Cui, Q.; Elstner, M. Semiempirical Quantum Mechanical Methods for Noncovalent Interactions for Chemical and Biochemical Applications. *Chem. Rev.* **2016**, *116*, 5301−5337.
(12) Riley, K. E.; Hobza, P. Noncovalent Interactions in Biochemistry. *Wiley Interdiscip. Rev.: Comput. Mol. Sci.* **2011**, *1*, 3−17.
(13) Jensen, F. How Large is the Elephant in the Density Functional Theory Room? *J. Phys. Chem. A* **2017**, *121*, 6104−6107.
(14) Mardirossian, N.; Head-Gordon, M. Thirty Years of Density Functional Theory in Computational Chemistry: An Overview and Extensive Assessment of 200 Density Functionals. *Mol. Phys.* **2017**, *115*, 2315−2372.
(15) Mosquera, M. A.; Fu, B.; Kohlstedt, K. L.; Schatz, G. C.; Ratner, M. A. Wave Functions, Density Functionals, and Artificial Intelligence for Materials and Energy Research: Future Prospects and Challenges. *ACS Energy Lett.* **2018**, *3*, 155−162.
(16) Jones, R. O. Density Functional Theory: Its Origins, Rise to Prominence, and Future. *Rev. Mod. Phys.* **2015**, *87*, 897−923.
(17) Becke, A. D. Perspective: Fifty Years of Density-Functional Theory in Chemical Physics. *J. Chem. Phys.* **2014**, *140*, 18A301.
(18) Kryachko, E. S.; Ludeña, E. V. Density Functional Theory: Foundations Reviewed. *Phys. Rep.* **2014**, *544*, 123−239.
(19) Körzdörfer, T.; Brédas, J.-L. Organic Electronic Materials: Recent Advances in the DFT Description of the Ground and Excited States Using Tuned Range-Separated Hybrid Functionals. *Acc. Chem. Res.* **2014**, *47*, 3284−3291.
(20) Peverati, R.; Truhlar, D. G. Quest for a Universal Density Functional: The Accuracy of Density Functionals across a Broad Spectrum of Databases in Chemistry and Physics. *Philos. Trans. R. Soc., A* **2014**, *372*, 20120476.
(21) DiLabio, G. A.; de-la Roza, A. O. *Reviews in Computational Chemistry*; John Wiley & Sons, Inc.: New York, 2016; pp 1−97.
(22) Zhang, Y. Molecular Spin on Surface: From Strong Correlation to Dispersion Interactions. *J. Chem. Phys.* **2016**, *145*, 124704.
(23) Johnson, E. R.; Mackie, I. D.; DiLabio, G. A. Dispersion interactions in density-functional theory. *J. Phys. Org. Chem.* **2009**, *22*, 1127.
(24) Perdew, J. P.; Wang, Y. Accurate and Simple Analytic Representation of the Electron-Gas Correlation Energy. *Phys. Rev. B: Condens. Matter Mater. Phys.* **1992**, *45*, 13244−13249.
(25) Perdew, J. P.; Burke, K.; Ernzerhof, M. Generalized Gradient Approximation Made Simple. *Phys. Rev. Lett.* **1996**, *77*, 3865−3868.
(26) Perdew, J. P.; Burke, K.; Ernzerhof, M. Errata: Generalized Gradient Approximation Made Simple. *Phys. Rev. Lett.* **1997**, *78*, 1396.
(27) Zhao, Y.; Truhlar, D. G. The M06 Suite of Density Functionals for Main Group Thermochemistry, Thermochemical Kinetics, Noncovalent Interactions, Excited States, and Transition Elements: Two New Functionals and Systematic Testing of Four M06-class Functionals and 12 Other Functionals. *Theor. Chem. Acc.* **2008**, *120*, 215−241.
(28) Becke, A. D. Density-Functional Thermochemistry. III. The Role of Exact Exchange. *J. Chem. Phys.* **1993**, *98*, 5648−5652.
(29) Otero-de-la-Roza, A.; Johnson, E. R. Many-Body Dispersion Interactions from the Exchange-Hole Dipole Moment Model. *J. Chem. Phys.* **2013**, *138*, 054103.
(30) Otero-de-la-Roza, A.; Johnson, E. R. A Benchmark for Non-Covalent Interactions in Solids. *J. Chem. Phys.* **2012**, *137*, 054103.
(31) Vincent, M. A.; Hillier, I. H.; Morgado, C. A.; Burton, N. A.; Shan, X. The Structure and Binding Energies of the van der Waals Complexes of Ar and N_2 with Phenol and its Cation, Studied by High Level Ab Initio and Density Functional Theory Calculations. *J. Chem. Phys.* **2008**, *128*, 044313.
(32) Johnson, E. R.; DiLabio, G. A. Structure and Binding Energies in van der Waals Dimers: Comparison between Density Functional Theory and Correlated Ab Initio Methods. *Chem. Phys. Lett.* **2006**, *419*, 333−339.
(33) Burns, L. A.; Vazquez-Mayagoitia, A.; Sumpter, B. G.; Sherrill, C. D. Density-Functional Approaches to Noncovalent Interactions: A Comparison of Dispersion Corrections (DFT-D), Exchange-Hole Dipole Moment (XDM) Theory, and Specialized Functionals. *J. Chem. Phys.* **2011**, *134*, 084107.
(34) Chai, J.-D.; Head-Gordon, M. Long-range Corrected Hybrid Density Functionals with Damped Atom-Atom Dispersion Corrections. *Phys. Chem. Chem. Phys.* **2008**, *10*, 6615.
(35) Chai, J.-D.; Head-Gordon, M. Systematic Optimization of Long-range Corrected Hybrid Density Functionals. *J. Chem. Phys.* **2008**, *128*, 084106.
(36) Grimme, S.; Ehrlich, S.; Goerigk, L. Effect of the Damping Function in Dispersion Corrected Density Functional Theory. *J. Comput. Chem.* **2011**, *32*, 1456−1465.
(37) Grimme, S.; Huenerbein, R.; Ehrlich, S. On the Importance of the Dispersion Energy for the Thermodynamics Stability of Molecules. *ChemPhysChem* **2011**, *12*, 1258−1261.
(38) Grimme, S.; Hansen, A.; Brandenburg, J. G.; Bannwarth, C. Dispersion-Corrected Mean-Field Electronic Structure Methods. *Chem. Rev.* **2016**, *116*, 5105.
(39) Hobza, P.; Řezáč, J. Introduction: Noncovalent Interactions. *Chem. Rev.* **2016**, *116*, 4911.
(40) Grimme, S. Accurate Description of van der Waals Complexes by Density Functional Theory including Empirical Corrections. *J. Comput. Chem.* **2004**, *25*, 1463−1473.
(41) Grimme, S. Semiempirical GGA-type Density Functional Constructed with a Long-range Dispersion Correction. *J. Comput. Chem.* **2006**, *27*, 1787−1799.
(42) Grimme, S.; Antony, J.; Ehrlich, S.; Krieg, H. A Consistent and Accurate Ab Initio Parametrization of Density Functional Dispersion Correction DFT-D) for the 94 Elements H-Pu. *J. Chem. Phys.* **2010**, *132*, 154104.
(43) Caldeweyher, E.; Ehlert, S.; Hansen, A.; Neugebauer, H.; Spicher, S.; Bannwarth, C.; Grimme, S. A Generally Applicable Atomic-Charge Dependent London Dispersion Correction. *J. Chem. Phys.* **2019**, *150*, 154122.
(44) Tkatchenko, A.; Scheffler, M. Accurate Molecular van Der Waals Interactions from Ground-State Electron Density and Free-Atom Reference Data. *Phys. Rev. Lett.* **2009**, *102*, 073005.
(45) Becke, A. D.; Johnson, E. R. Exchange-Hole Dipole Moment and the Dispersion Interaction. *J. Chem. Phys.* **2005**, *122*, 154104.
(46) Dion, M.; Rydberg, H.; Schröder, E.; Langreth, D. C.; Lundqvist, B. I. Van der Waals Density Functional for General Geometries. *Phys. Rev. Lett.* **2004**, *92*, 246401.
(47) Lee, K.; Murray, E. D.; Kong, L.; Lundqvist, B. I.; Langreth, D. C. Higher-Accuracy van der Waals Density Functional. *Phys. Rev. B: Condens. Matter Mater. Phys.* **2010**, *82*, 081101.
(48) Callsen, M.; Hamada, I. Assessing the Accuracy of the van der Waals Density Functionals for Rare-Gas and Small Molecular Systems. *Phys. Rev. B: Condens. Matter Mater. Phys.* **2015**, *91*, 195103.

https://dx.doi.org/10.1021/acs.jpca.9b10357
J. Phys. Chem. A 2020, 124, 1619−1633

(49) Vydrov, O. A.; Van Voorhis, T. Nonlocal van der Waals Density Functional Made Simple. *Phys. Rev. Lett.* **2009**, *103*, 063004.
(50) Vydrov, O. A.; Van Voorhis, T. Dispersion Interactions from a Local Polarizability Model. *Phys. Rev. A: At., Mol., Opt. Phys.* **2010**, *81*, 062708.
(51) Zhao, Y.; Truhlar, D. G. Exploring the Limit of Accuracy of the Global Hybrid Meta Density Functional for Main-Group Thermochemistry, Kinetics, and Noncovalent Interactions. *J. Chem. Theory Comput.* **2008**, *4*, 1849−1868.
(52) Peverati, R.; Truhlar, D. G. Improving the Accuracy of Hybrid Meta-GGA Density Functionals by Range Separation. *J. Phys. Chem. Lett.* **2011**, *2*, 2810−2817.
(53) Peverati, R.; Truhlar, D. G. M11-L: ALocal Density Functional That Provides Improved Accuracy for Electronic Structure Calculations in Chemistry and Physics. *J. Phys. Chem. Lett.* **2012**, *3*, 117−124.
(54) Peverati, R.; Truhlar, D. G. An Improved and Broadly Accurate Local Approximation to the Exchange-Correlation Density Functional: The MN12-L Functional for Electronic Structure Calculations in Chemistry and Physics. *Phys. Chem. Chem. Phys.* **2012**, *14*, 13171.
(55) Peverati, R.; Truhlar, D. G. Exchange-Correlation Functional with Good Accuracy for Both Structural and Energetic Properties while Depending Only on the Density and Its Gradient. *J. Chem. Theory Comput.* **2012**, *8*, 2310−2319.
(56) Peverati, R.; Truhlar, D. G. Screened-Exchange Density Functionals with Broad Accuracy for Chemistry and Solid-State Physics. *Phys. Chem. Chem. Phys.* **2012**, *14*, 16187.
(57) Lin, I.-C.; Coutinho-Neto, M. D.; Felsenheimer, C.; von Lilienfeld, O. A.; Tavernelli, I.; Rothlisberger, U. Library of Dispersion-Corrected Atom-Centered Potentials for Generalized Gradient Approximation Functionals: Elements H, C, N, O, He, Ne, Ar, and Kr. *Phys. Rev. B: Condens. Matter Mater. Phys.* **2007**, *75*, 205131.
(58) Otero-de-la-Roza, A.; DiLabio, G. A. Transferable Atom-Centered Potentials for the Correction of Basis Set Incompleteness Errors in Density-Functional Theory. *J. Chem. Theory Comput.* **2017**, *13*, 3505−3524.
(59) Prasad, V. K.; Otero-de-la-Roza, A.; DiLabio, G. A. Atom-Centered Potentials with Dispersion-Corrected Minimal-Basis-Set Hartree-Fock: An Efficient and Accurate Computational Approach for Large Molecular Systems. *J. Chem. Theory Comput.* **2018**, *14*, 726−738.
(60) van Santen, J. A.; DiLabio, G. A. Dispersion Corrections Improve the Accuracy of Both Noncovalent and Covalent Interactions Energies Predicted by a Density-Functional Theory Approximation. *J. Phys. Chem. A* **2015**, *119*, 6703−6713.
(61) Krukau, A. V.; Vydrov, O. A.; Izmaylov, A. F.; Scuseria, G. E. Influence of the Exchange Screening Parameter on the Performance of Screened Hybrid Functionals. *J. Chem. Phys.* **2006**, *125*, 224106.
(62) Schimka, L.; Harl, J.; Kresse, G. Improved Hybrid Functional for Solids: The HSEsol Functional. *J. Chem. Phys.* **2011**, *134*, 024116.
(63) Perdew, J. P.; Ruzsinszky, A.; Csonka, G. I.; Vydrov, O. A.; Scuseria, G. E.; Constantin, L. A.; Zhou, X.; Burke, K. Restoring the Density-Gradient Expansion for Exchange in Solids and Surfaces. *Phys. Rev. Lett.* **2008**, *100*, 136406.
(64) Becke, A. D. Density-Functional Thermochemistry. V. Systematic Optimization of Exchange-Correlation Functionals. *J. Chem. Phys.* **1997**, *107*, 8554−8560.
(65) Goerigk, L.; Hansen, A.; Bauer, C.; Ehrlich, S.; Najibi, A.; Grimme, S. A Look at the Density Functional Theory Zoo with the Advanced GMTKN55 Database for General Main Group Thermochemistry, Kinetics and Noncovalent Interactions. *Phys. Chem. Chem. Phys.* **2017**, *19*, 32184−32215.
(66) Hermann, J.; DiStasio, R. A.; Tkatchenko, A. First-Principles Models for van der Waals Interactions in Molecules and Materials: Concepts, Theory, and Applications. *Chem. Rev.* **2017**, *117*, 4714−4758.
(67) Kim, M.; Kim, W. J.; Lee, E. K.; Lebègue, S.; Kim, H. Recent Development of Atom-Pairwise van der Waals Corrections for Density Functional Theory: From Molecules to Solids. *Int. J. Quantum Chem.* **2016**, *116*, 598−607.
(68) Bučko, T.; Lebègue, S.; Hafner, J.; Ángyán, J. G. Improved Density Dependent Correction for the Description of London Dispersion Forces. *J. Chem. Theory Comput.* **2013**, *9*, 4293−4299.
(69) Mason, S. E.; Beton, P. H.; Besley, N. A. AIRBED: A Simplified Density Functional Theory Model for Physisorption on Surfaces. *J. Chem. Theory Comput.* **2019**, *15*, 5628−5634.
(70) Smith, D. G. A.; Burns, L. A.; Patkowski, K.; Sherrill, C. D. Revised Damping Parameters for the D3 Dispersion Correction to Density Functional Theory. *J. Phys. Chem. Lett.* **2016**, *7*, 2197−2203.
(71) Ucak, U. V.; Ji, H.; Singh, Y.; Jung, Y. A Soft Damping Function for Dispersion Corrections with Less Overfitting. *J. Chem. Phys.* **2016**, *145*, 174104.
(72) Bučko, T.; Hafner, J.; Lebégue, S.; Ángyán, J. G. Improved Description of the Structure of Molecular and Layered Crystals: Ab Initio DFT Calculations with van der Waals Corrections. *J. Phys. Chem. A* **2010**, *114*, 11814−11824.
(73) Civalleri, B.; Zicovich-Wilson, C. M.; Valenzano, L.; Ugliengo, P. B3LYP Augmented with an Empirical Dispersion Term (B3LYP-D*) as Applied to Molecular Crystals. *CrystEngComm* **2008**, *10*, 405−410.
(74) Tao, Y.; Zou, W.; Sethio, D.; Verma, N.; Qiu, Y.; Tian, C.; Cremer, D.; Kraka, E. In Situ Measure of Intrinsic Bond Strength in Crystalline Structures: Local Vibrational Mode Theory for Periodic Systems. *J. Chem. Theory Comput.* **2019**, *15*, 1761−1776.
(75) Feng, S.; Li, T. Predicting Lattice Energy of Organic Crystals by Density Functional Theory with Empirically Corrected Dispersion Energy. *J. Chem. Theory Comput.* **2006**, *2*, 149−156.
(76) Zhang, J.; Riesen, H. Controlled Generation of Tm^{2+} Ions in Nanocrystalline BaFCl:Tm^{3+} by X-ray Irradiation. *J. Phys. Chem. A* **2017**, *121*, 803−809.
(77) Liu, Z.; Stevens-Kalceff, M.; Riesen, H. Photoluminescence and Cathodoluminescence Properties of Nanocrystalline BaFCl:Sm^{3+} X-ray Storage Phosphor. *J. Phys. Chem. C* **2012**, *116*, 8322−8331.
(78) Riesen, H.; Kaczmarek, W. A. Efficient X-ray Generation of Sm^{2+} in Nanocrystalline BaFCl/Sm^{3+}: A Photoluminescent X-ray Storage Phosphor. *Inorg. Chem.* **2007**, *46*, 7235−7237.
(79) Liu, B.; Shi, C.; Yin, M.; Fu, Y.; Shen, D. Electronic, Optical and Luminescent Properties of PbFCl Single Crystal. *J. Phys.: Condens. Matter* **2005**, *17*, 5087.
(80) Chen, J.; Shen, D.; Ren, G.; Mao, R.; Yin, Z. A High-Density Inorganic Scintillator: Lead Fluoride Chloride. *J. Phys. D: Appl. Phys.* **2004**, *37*, 938−941.
(81) Comodi, P.; Zanazzi, P. F. Improved Calibtration Curve for the Sm^{2+}:BaFCl Pressure Sensor. *J. Appl. Crystallogr.* **1993**, *26*, 843−845.
(82) Riesen, H.; Badek, K.; Monro, T. M.; Riesen, N. Highly Efficient Valence State Switching of Samarium in BaFCl:Sm Nanocrystals in the Deep UV for Multilevel Optical Data Storage. *Opt. Mater. Express* **2016**, *6*, 3097−3108.
(83) Sorb, Y.; Sornadurai, D. Structural Phase Transitions of Ionic Layered PbFX (X = Cl or Br) Compounds under High Pressure. *Mater. Res. Bull.* **2015**, *65*, 1−6.
(84) Bourret-Courchesne, E.; Bizarri, G.; Borade, R.; Gundiah, G.; Samulon, E.; Yan, Z.; Derenzo, S. Crystal Growth and Characterization of Alkali-Earth Halide Scintillators. *J. Cryst. Growth* **2012**, *352*, 78−83.
(85) Yedukondalu, N.; Babu, K. R.; Bheemalingam, C.; Singh, D. J.; Vaitheeswaran, G.; Kanchana, V. Electronic Structure, Optical Properties, and Bonding in Alkaline-Earth Halofluoride Scintillators: BaClF, BaBrF, and BaIF. *Phys. Rev. B: Condens. Matter Mater. Phys.* **2011**, *83*, 165117.
(86) Yedukondalu, N.; Esfahani, M. M. D. Unraveling the Hidden Martensitic Phase Transition in BaClF and PbClF under High Pressure Using an Ab Initio Evolutionary Approach. *Inorg. Chem.* **2019**, *58*, 5886−5899.
(87) Rajan, K. G.; Lenus, A. J. X-ray Excited Optical Luminescence Studies on the System BaXY (X,Y = F, Cl, Br, I). *Pramana* **2005**, *65*, 323−338.
(88) Kushwaha, A. K.; Akbudak, S.; Yadav, A. C.; Uğur, Ş.; Uğur, G. Lattice dynamical and elastic properties of BaFX (X = Cl, Br and I): Matlockite structure compounds. *Int. J. Mod. Phys. B* **2019**, *33*, 1950221.

(89) Sorb, Y. A.; Subramanian, N.; Ravindran, T. R. High Pressure Raman Spectroscopy of Layered Matlockite, PbFCl. *J. Phys.: Condens. Matter* **2013**, *25*, 155401.
(90) Zhang, G.-X.; Reilly, A. M.; Tkatchenko, A.; Scheffler, M. Performance of Various Density-Functional Approximations for Cohesive Properties of 64 Bulk Solids. *New J. Phys.* **2018**, *20*, 063020.
(91) Lejaeghere, K.; Van Speybroeck, V.; Van Oost, G.; Cottenier, S. Error Estimates for Solid-State Density-Functional Theory Predictions: An Overview by Means of the Ground-State Elemental Crystals. *Crit. Rev. Solid State Mater. Sci.* **2014**, *39*, 1−24.
(92) Berland, K.; Cooper, V. R.; Lee, K.; Schröder, E.; Thonhauser, T.; Hyldgaard, P.; Lundqvist, B. I. van der Waals Forces in Density Functional Theory: A Review of the vdW-DF Method. *Rep. Prog. Phys.* **2015**, *78*, 066501.
(93) Björkman, T.; Gulans, A.; Krasheninnikov, A. V.; Nieminen, R. M. van der Waals Bonding in Layered Compounds from Advanced Density-Functional First-Principles Calculations. *Phys. Rev. Lett.* **2012**, *108*, 235502.
(94) Shalaev, A.; Shendrik, R.; Myasnikova, A.; Bogdanov, A.; Rusakov, A.; Vasilkovskyi, A. Luminescence of BaBrI and SrBrI Single Crystals Doped with Eu^{2+}. *Opt. Mater.* **2018**, *79*, 84−89.
(95) D'Anna, V.; Daku, L. M. L.; Hagemann, H.; Kubel, F. Ionic Layered BaFCl and $Ba_{1-x}Sr_xFCI$ Compounds: Physical- and Chemical-Pressure Effects. *Phys. Rev. B: Condens. Matter Mater. Phys.* **2010**, *82*, 024108.
(96) Sethio, D. Critical Evaluation of the Effect of Anharmonicity and Dispersion Interactions using Density Functional Theory on Structural and Spectroscopic Properties of Selected Inorganic Compounds. *Ph.D. Dissertation*, University of Geneva, Geneva, Switzerland, 2017.
(97) Kanchana, V.; Yedukondalu, N.; Vaitheeswaran, G. Structural, Elastic, Electronic and Optical Properties of Layered Alkaline-Earth Halofluoride Scintillators. *Philos. Mag.* **2013**, *93*, 3563−3575.
(98) Reshak, A. H.; Charifi, Z.; Baaziz, H. Optical Properties of the Alkaline-Earth Fluorohalides Matlockite-type Structure SrFX (X = Cl, Br, I) Compounds. *Phys. B* **2008**, *403*, 711−716.
(99) Su, N. Q.; Adamo, C.; Xu, X. A Comparison of Geometric Parameters from PBE-based Doubly Hybrid Density Functionals PBE0-DH, PBE0−2, and xDH-PBE0. *J. Chem. Phys.* **2013**, *139*, 174106.
(100) Bühl, M.; Reimann, C.; Pantazis, D. A.; Bredow, T.; Neese, F. Geometries of Third-Row Transition-Metal Complexes from Density-Functional Theory. *J. Chem. Theory Comput.* **2008**, *4*, 1449−1459.
(101) Xu, X.; Goddard, W. A. The Extended Perdew-Burke-Ernzerhof Functional with Improved Accuracy for Thermodynamic and Electronic Properties of Molecular Systems. *J. Chem. Phys.* **2004**, *121*, 4068−4082.
(102) Ernzerhof, M.; Scuseria, G. E. Assessment of the Perdew-Burke-Ernzerhof Exchange-Correlation Functional. *J. Chem. Phys.* **1999**, *110*, 5029−5036.
(103) Peintinger, M. F.; Oliveira, D. V.; Bredow, T. Consistent Gaussian Basis Sets of Triple-zeta Valence with Polarization Quality for Solid-state Calculations. *J. Comput. Chem.* **2013**, *34*, 451−459.
(104) Weigend, F.; Häser, M.; Patzelt, H.; Ahlrichs, R. RI-MP2: Optimized Auxiliary Basis Sets and Demonstration of Efficiency. *Chem. Phys. Lett.* **1998**, *294*, 143−152.
(105) Weigend, F.; Ahlrichs, R. Balanced Basis Sets of Split Valence, Triple Zeta Valence and Quadruple Zeta Valence Quality for H to Rn: Design and Assessment of Accuracy. *Phys. Chem. Chem. Phys.* **2005**, *7*, 3297−3305.
(106) Laun, J.; Oliveira, D. V.; Bredow, T. Consistent Gaussian Basis Sets of Double- and Triple-Zeta Valence with Polarization Quality of the Fifth Period for Solid-State Calculations. *J. Comput. Chem.* **2018**, *39*, 1285−1290.
(107) Towler, M. *CRYSTAL*; University of Cambridge, http://www.tcm.phy.cam.ac.uk/~mdt26/crystal.html (last accessed: August 22, 2019).
(108) Wu, Q.; Yang, W. Empirical Correction to Density Functional Theory for van der Waals Interactions. *J. Chem. Phys.* **2002**, *116*, 515−524.
(109) Perdew, J. P.; Burke, K.; Ernzerhof, M. Generalized Gradient Approximation Made Simple [Phys. Rev. Lett. 77, 3865 (1996)]. *Phys. Rev. Lett.* **1997**, *78*, 1396−1396.
(110) Adamo, C.; Barone, V. Toward Reliable Density Functional Methods without Adjustable Parameters: The PBE0Model. *J. Chem. Phys.* **1999**, *110*, 6158−6170.
(111) Kerber, T.; Sierka, M.; Sauer, J. Application of Semiempirical Long-Range Dispersion Corrections to Periodic Systems in Density Functional Theory. *J. Comput. Chem.* **2008**, *29*, 2088−2097.
(112) Svelle, S.; Tuma, C.; Rozanska, X.; Kerber, T.; Sauer, J. Quantum Chemical Modeling of Zeolite-Catalyzed Methylation Reactions: Toward Chemical Accuracy for Barriers. *J. Am. Chem. Soc.* **2009**, *131*, 816−825.
(113) Tosoni, S.; Sauer, J. Accurate Quantum Chemical Energies for the Interaction of Hydrocarbons with Oxide Surfaces: CH_4/MgO-(001). *Phys. Chem. Chem. Phys.* **2010**, *12*, 14330.
(114) Andersson, M. P. Density Functional Theory with Modified Dispersion Correction for Metals Applied to Molecular Adsorption on Pt(111). *Phys. Chem. Chem. Phys.* **2016**, *18*, 19118−19122.
(115) Andersson, M. P. Density Functional Theory with Modified Dispersion Correction for Metals Applied to Self-Assembled Monolayers of Thiols on Au(111). *J. Theor. Chem.* **2013**, *2013*, 1−9.
(116) Dovesi, R.; Orlando, R.; Erba, A.; Zicovich-Wilson, C. M.; Civalleri, B.; Casassa, S.; Maschio, L.; Ferrabone, M.; De La Pierre, M.; D'Arco, P.; et al. CRYSTAL14: A Program for the Ab Initio Investigation of Crystalline Solids. *Int. J. Quantum Chem.* **2014**, *114*, 1287−1317.
(117) Monkhorst, H. J.; Pack, J. D. Special Points for Brillouin-zone Integrations. *Phys. Rev. B* **1976**, *13*, 5188−5192.
(118) Nieuwenkamp, W.; Bijvoet, J. M. Die Kristallstruktur von Bleifluochlorid PbFCl. *Z. Kristallogr. - Cryst. Mater.* **1932**, *81*, 469.
(119) Sauvage, M. Refinement of the Structures of SrFCl and BaFCl. *Acta Crystallogr., Sect. B: Struct. Crystallogr. Cryst. Chem.* **1974**, *30*, 2786−2787.
(120) Dovesi, R.; Erba, A.; Orlando, R.; Zicovich-Wilson, C. M.; Civalleri, B.; Maschio, L.; Rérat, M.; Casassa, S.; Baima, J.; Salustro, S.; et al. Quantum-Mechanical Condensed Matter Simulations with CRYSTAL. *WIREs Comput. Mol. Sci.* **2018**, *8*, e1360.
(121) Blöchl, P. E. Projector Augmented-Wave Method. *Phys. Rev. B: Condens. Matter Mater. Phys.* **1994**, *50*, 17953−17979.
(122) Kresse, G.; Joubert, D. From Ultrasoft Pseudopotentials to the Projector Augmented-Wave Method. *Phys. Rev. B: Condens. Matter Mater. Phys.* **1999**, *59*, 1758−1775.
(123) Kresse, G.; Hafner, J. Ab Initio Molecular Dynamics for Liquid Metals. *Phys. Rev. B: Condens. Matter Mater. Phys.* **1993**, *47*, 558.
(124) Kresse, G.; Hafner, J. Ab Initio Molecular Dynamics for Liquid Metals. *Phys. Rev. B: Condens. Matter Mater. Phys.* **1993**, *47*, 558.
(125) Kresse, G.; Furthmüller, J. Efficient Iterative Schemes for Ab Initio Total-Energy Calculations using a Plane-Wave Basis Set. *Phys. Rev. B: Condens. Matter Mater. Phys.* **1996**, *54*, 11169−11186.
(126) Kresse, G.; Furthmüller, J. Efficiency of Ab-Initio Total Energy Calculations For Metals and Semiconductors Using a Plane-Wave Basis Set. *Comput. Mater. Sci.* **1996**, *6*, 15−50.
(127) Hafner, J. Ab Initio Simulations of Materials using VASP: Density-Functional Theory and Beyond. *J. Comput. Chem.* **2008**, *29*, 2044−2078.
(128) Giannozzi, P.; Baroni, S.; Bonini, N.; Calandra, M.; Car, R.; Cavazzoni, C.; Ceresoli, D.; Chiarotti, G. L.; Cococcioni, M.; Dabo, I.; et al. QUANTUM ESPRESSO: A Modular and Open-Source Software Project for Quantum Simulations of Materials. *J. Phys.: Condens. Matter* **2009**, *21*, 395502.
(129) Giannozzi, P.; Andreussi, O.; Brumme, T.; Bunau, O.; Nardelli, M. B.; Calandra, M.; Car, R.; Cavazzoni, C.; Ceresoli, D.; Cococcioni, M.; et al. Advanced Capabilities for Materials Modelling with Quantum ESPRESSO. *J. Phys.: Condens. Matter* **2017**, *29*, 465901.
(130) To be published, University of Geneva.
(131) Beck, H. P. A Study on Mixed Halide Compounds MFX (M = Ca, Sr, Eu, Ba; X = Cl, Br, I). *J. Solid State Chem.* **1976**, *17*, 275.

https://dx.doi.org/10.1021/acs.jpca.9b10357
J. Phys. Chem. A 2020, 124, 1619−1633

(132) Hagemann, H.; D'Anna, V.; Lawson Daku, L. M.; Kubel, F. Crystal Chemistry in Barium Flouride Chloride System. *Cryst. Growth Des.* **2012**, *12*, 1124.
(133) Liebich, B. W.; Nicollin, D. Refinement of the PbFCl Types BaFI, BaFBr, and CaFCl. *Acta Crystallogr., Sect. B: Struct. Crystallogr. Cryst. Chem.* **1977**, *33*, 2790.
(134) Pasero, M.; Perchiazzi, M. Crystal Structure Refinement of Matlockite. *Mineral. Mag.* **1996**, *60*, 833.
(135) Sundarakkannan, B.; Kesavamoorthy, R. Anharmonic Behaviour of BaFCl using Raman Scattering. *Eur. Phys. J. B* **1998**, *3*, 179−183.
(136) De La Pierre, M.; Orlando, R.; Maschio, L.; Doll, K.; Ugliengo, P.; Dovesi, R. Performance of Six Functionals (LDA, PBE, PBESOL, B3LYP, PBE0, and WC1LYP) in the Simulation of Vibrational and Dielectric Properties of Crystalline Compounds. The Case of Forsterite Mg_2SiO_4. *J. Comput. Chem.* **2011**, *32*, 1775−1784.
(137) Demichelis, R.; Civalleri, B.; Ferrabone, M.; Dovesi, R. On the Performance of Eleven DFT Functionals in the Description of the Vibrational Properties of Aluminosilicates. *Int. J. Quantum Chem.* **2010**, *110*, 406−415.
(138) Nicollin, D.; Bill, H. Experimental Contribution to the Study of S-state Ions in Ionic Single Crystals. *J. Phys. C: Solid State Phys.* **1978**, *11*, 4803.
(139) Sieskind, M.; Ayadi, M.; Zachmann, G. Infrared Lattice Vibration, Dielectric Dispersion, and Lattice Dynamics of BaFCl. *Phys. Status Solidi B* **1986**, *136*, 489−495.
(140) Rulmont, A. Spectres Infrarouges et Raman des Fluorohalogénures de Plumb PBPX (X = Cl, Br, I). *Spectrochim. Acta A: Mol. Spect.* **1974**, *30*, 161−168.
(141) Hagemann, H.; Rief, A.; Kubel, F.; van Mechelen, J. L. M.; Tran, F.; Blaha, P. Mixed $PbFBr_{1-x}I_x$ Crystals: Structural and Spectroscopic Investigations. *J. Phys.: Condens. Matter* **2007**, *19*, 036214.
(142) Shen, Y. R.; Englisch, U.; Chudinovskikh, L.; Porsch, F.; Haberkorn, R.; Beck, H. P.; Holzapfel, W. B. A Structural Study on the PbFCl-type Compounds MFCl (M = Ba, Sr and and BaFBr under High Pressure. *J. Phys.: Condens. Matter* **1994**, *6*, 3197−3206.
(143) Decremps, F.; Gauthier, M.; Chervin, J.-C.; Fischer, M.; Polian, A. Unexpected Value of Transition Pressure in the Ionic Layered BaFI Compound Observed by Raman Scattering. *Phys. Rev. B: Condens. Matter Mater. Phys.* **2002**, *66*, 024115.
(144) Oliveira, V.; Kraka, E.; Cremer, D. The Intrinsic Strength of the Halogen Bond: Electrostatic and Covalent Contributions Described by Coupled Cluster Theory. *Phys. Chem. Chem. Phys.* **2016**, *18*, 33031−33046.
(145) Oliveira, V.; Kraka, E.; Cremer, D. Quantitative Assessment of Halogen Bonding Utilizing Vibrational Spectroscopy. *Inorg. Chem.* **2017**, *56*, 488−502.
(146) Oliveira, V.; Cremer, D. Transition from Metal-Ligand Bonding to Halogen Bonding Involving a Metal as Halogen Acceptor: A Study of Cu, Ag, Au, Pt, and Hg Complexes. *Chem. Phys. Lett.* **2017**, *681*, 56−63.
(147) Oliveira, V.; Kraka, E. Systematic Coupled Cluster Study of Noncovalent Interactions Involving Halogens, Chalcogens, and Pnicogens. *J. Phys. Chem. A* **2017**, *121*, 9544−9556.

https://dx.doi.org/10.1021/acs.jpca.9b10357
J. Phys. Chem. A 2020, 124, 1619−1633